Supporting Information

Structure-Based Discovery of Novel Cyclophillin A Inhibitors for the Treatment of Hepatitis C Virus Infections

Suhui Yang,[†,#,⊥] Jyothi K.R.,[‡,#] Sangbin Lim,[‡] Tae Gyu Choi,[‡] Jin-Hwan Kim,[‡] Salima Akter,[‡] Miran Jang,[‡] Hyun-Jong Ahn,[∥] Hee-Young Kim,[⊥] Marc P. Windisch,[⊥] Daulat B. Khadka,[†] Chao Zhao,[†] Yifeng Jin,[†] Insug Kang,[‡] Joohun Ha,[‡] Byung-Chul Oh,[¶] Meehyein Kim,[○] Sung Soo Kim[‡,*] and Won-Jea Cho[†,*]

[†]College of Pharmacy and Research Institute of Drug Development, Chonnam National University, Gwangju 500-757, Republic of Korea

[‡]Department of Biochemistry and Molecular Biology, School of Medicine, Kyung Hee University, Seoul 130-701, Republic of Korea

[∥]Department of Microbiology, School of Medicine, Kyung Hee University, Seoul 130-701, Republic of Korea

[⊥]Applied Molecular Virology, Institut Pasteur Korea, Gyeonggi-do 463-400, Republic of Korea

[¶]Lee Gil Ya Cancer and Diabetes Institute, Gachon University of Medicine and Science, Incheon 406-840, Republic of Korea

[○]Virus Research and Testing Group, Korea Research Institute of Chemical Technology, Daejeon 305-600, Republic of Korea

*To whom correspondence should be addressed:

Won-Jea Cho, Ph.D., Phone: +82-62-530-2911. Fax: +82-62-530-2911. E-mail: wjcho@jnu.ac.kr.
Sung Soo Kim, Ph.D., Phone: +82-2-961-0524. Fax: +82-2-959-8168. E-mail: sgskim@khu.ac.kr.

[#]These authors contributed equally.

[⊥] Present address: Department of Medicinal Chemistry, College of Pharmacy, Translational Oncology Program, University of Michigan, North Campus Research Complex, Bldg 520, Ann Arbor, MI 48109, United States.

Table of Contents

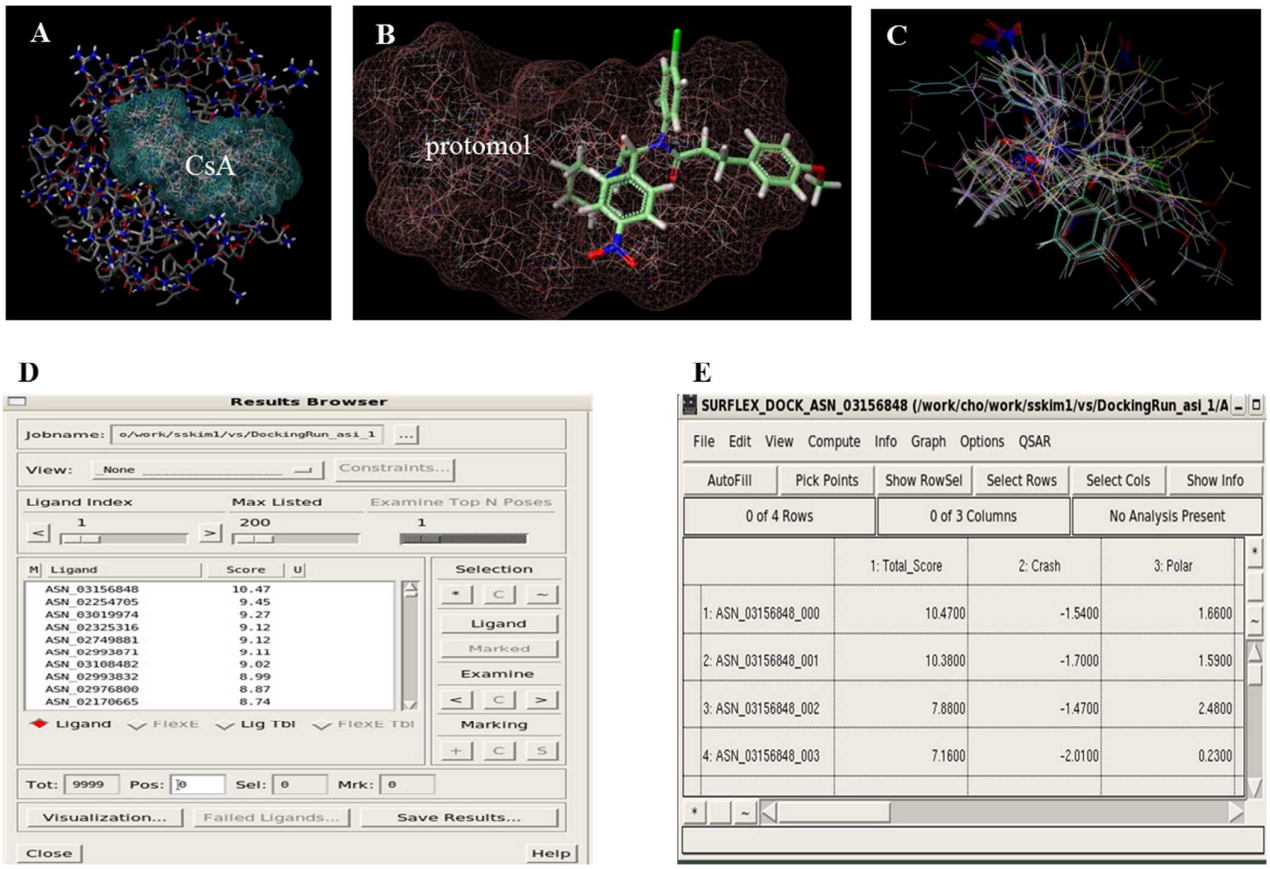

Figure S1. Virtual screening process. (A) X-ray structure of CypA and CsA. Categorization of protein active site, construction of docking target to match molecules and production of a protomol. (B) The model uses a pseudomolecule as the target to align assumed ligands of a protein's binding site. In this research, ligand-based protomol generation was applied. (C) The hit structure obtained after virtual screening are superimposed in the molecular areas. (D) Virtual screening results; ranking the hit compounds on the basis of the docking scores. (E) Three scores for each docked conformation are applied: a nominal affinity that is considered to be the total score (log(Kd)), a crash score (also pKd units), and the portion of the total score that resulted from polar interactions.

Table S1. List of isocyanides (**1**), aldehydes (**2**), amines (**3**) and carboxylic acids (**4**).

Isocyanide (R^1-NC)	Aldehyde (R^2-CHO)	Amine (R^3-NH_2)	Carboxylic acid (R^4-COOH)
1a: 	**2a**: 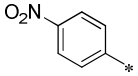	**3a**: 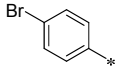	**4a**: 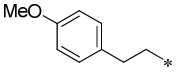
1b: 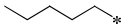	**2b**: 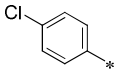	**3b**: 	**4b**: 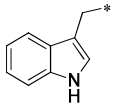
2c: 	**3c**: 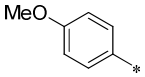	**4c**: 	
2d: 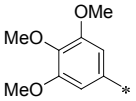	**3d**: 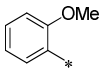	**4d**: 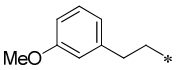	
2e: 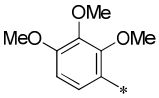	**3e**: 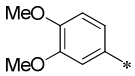	**4e**: 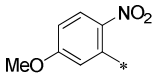	
2f: 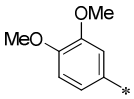	**3f**: 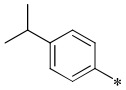	**4f**: 	
2g: 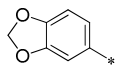	**3g**: 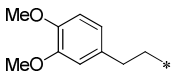	**4g** 	
2h: 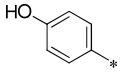	**3h**: 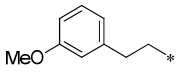	**4h** 	
2i: 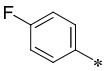		**4i** 	
		4j 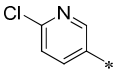	

Optimization of Ugi reaction

Reaction parameters such as temperature, solvent and microwave irradiation were investigated to find out the optimum conditions for better yield and easy purification of final product. Similar chemical yields of the Ugi product were obtained regardless of changes in temperature, but prolonged heating was likely to decrease the yield to some extent (Data not shown). With regard to solvents, polar protic solvents such as 2,2,2-trifluoroethanol (TFE) generally resulted in higher yield when compared to polar aprotic or non-polar solvents (Table S2). Considering the high solubility of the reactant and low solubility of Ugi product which in turn make the purification step easier, we chose to use polar protic solvents for synthesis of bis-amides. Moreover, we confirmed that microwave irradiation led to an impressive shortening of the reaction time as reported[1] and higher yields compared to conventional methodology (Table S3).

Table S2. Comparison of synthetic yields of bis-amide **14** by applying different solvents.

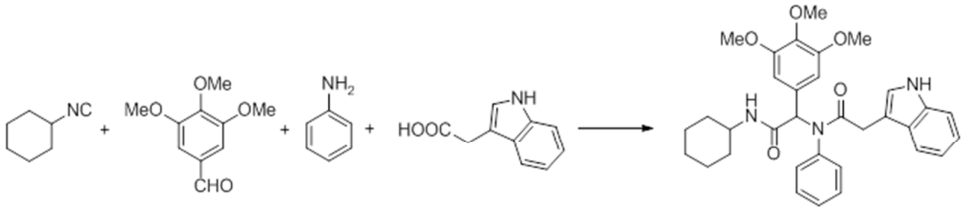

Solvent	Polar protic		Polar aprotic		Non-polar	
	TFE[a]	MeOH	EtOH	MeCN	EtOAc	THF[b]
Yield (%)	55	43	34	51	4	26

[a] 2,2,2-Trifluoroethanol, [b] Tetrahydrofuran

Table S3. Comparison of synthetic yields of bis-amide **26** by applying microwave irradiation or room temperature.

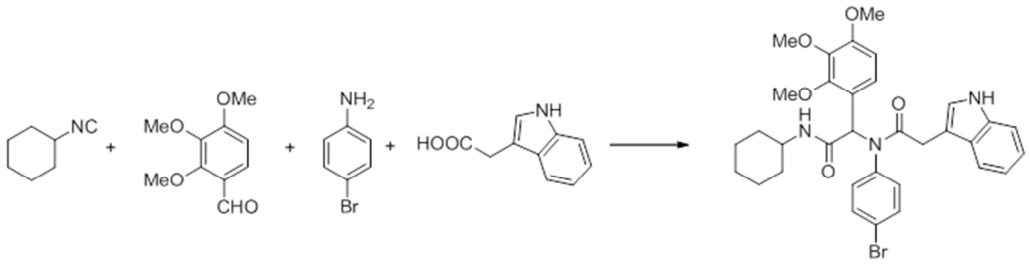

Rxn Condition	Rxn Time	Yield (%)
μw, 100 W, 60 °C	40 min	77
rt	48 h	50

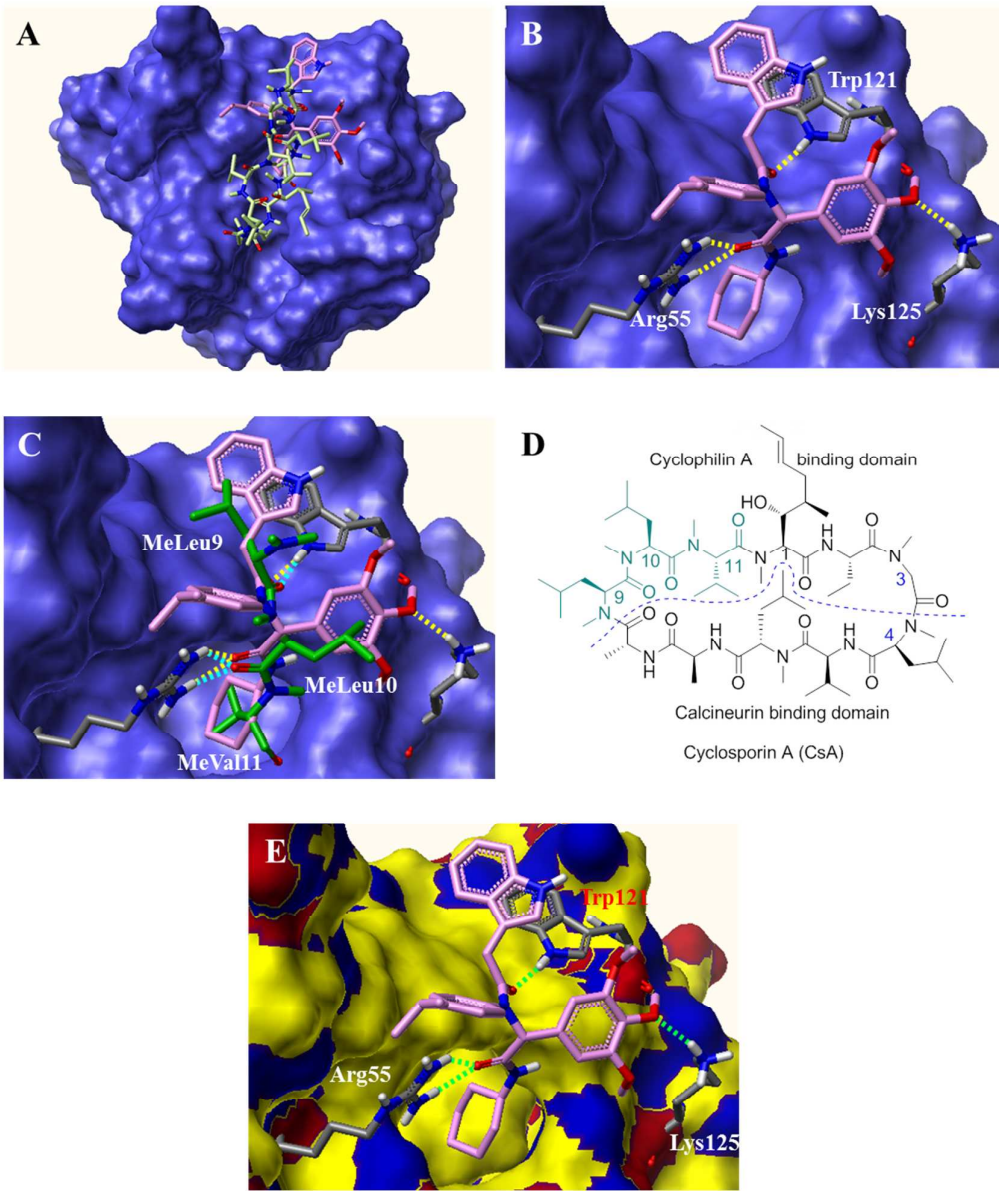

Figure S2. Low-energy binding conformation of **25** and CsA bound to CypA. (A) Overview of CsA (light green) and lead (**25**, lavender) bound to the surface of CypA (dark blue) along a groove. (B) Binding mode of **25** and CypA. Cyclohexyl group is merged inside a cavity which consists of Phe113 as a base. The amides, C=O of **25** associates with Arg55 and Trp121, and oxygen of trimethoxyphenyl group interacts with Lys125 by hydrogen bonds (yellow dotted lines). Indolymethyl group overlays over Trp121. (C) Identical H-bond interactions of CsA (green, only 3 amino acid units are shown) and **25** (lavender) with CypA; light blue and yellow dotted lines repesent H-bonds of CsA and **25** with CypA, respectivley. (D) Structure of CsA showing CypA and calcineurin bindng domains (separated by blue dashed line) and residues (green colored) that overlap with docked bis-amides. (E) H-bonding and hydrophobic regions of CypA; region occupied by hydrophobic moiety is yellow, by H-bond donor is blue and by H-bond acceptor is red. Hydrophobic cyclohexyl and isopropylphenyl groups are well situated in the hydrophobic regions. H-bonds are displayed as green dotted lines.

Isothermal titration calorimetry

The isothermal titration calorimetry (ITC) data for the binding of **25** to CypA are shown in Figure S3. For **25**, a reasonable fit was achieved with a two-site set model in which **25** binds one site with high affinity and another with low affinity. This may be due to the mixture of soluble cyclophilin A and insoluble one because of high concentration of EtOH in the reaction mixtures.

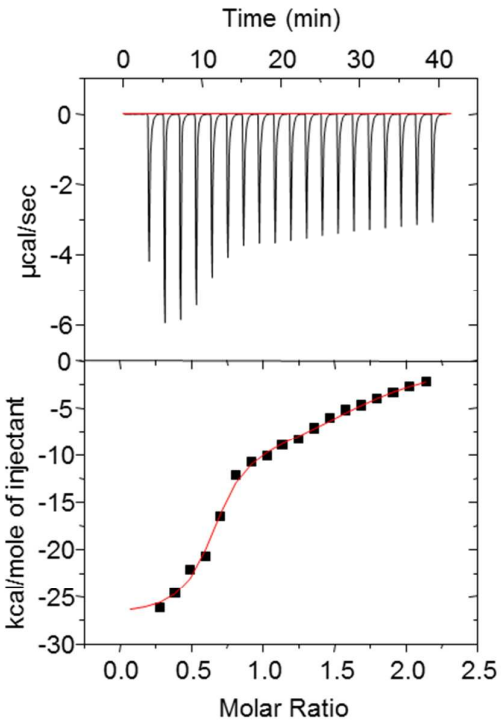

Figure S3. ITC analysis of **25** binding to CypA. The data relating to the heat changes that accompany the binding of **25** to CypA are shown in the upper panel. The binding isotherms, which correspond to plots of integrated heat as a function of the molar ration of **25**:CypA, are shown in the lower panel.

Table S4. Thermodynamic parameters of **25** binding to CypA determined by ITC.

Parameter	
K_{d1} (10^{-6} M)	7.69
n_1	1.06
ΔG_1 (cal/mol^{-1})	2,608
ΔH_1 (cal/mol^{-1})	-1,050
ΔS_1 (cal/mol/deg^{-1})	-11.8
K_{d2} (10^{-6} M)	0.15
n_2	0.60
ΔG_2 (cal/mol^{-1})	15,795
ΔH_2 (cal/mol^{-1})	-2,712
ΔS_2 (cal/mol/deg^{-1})	-59.7

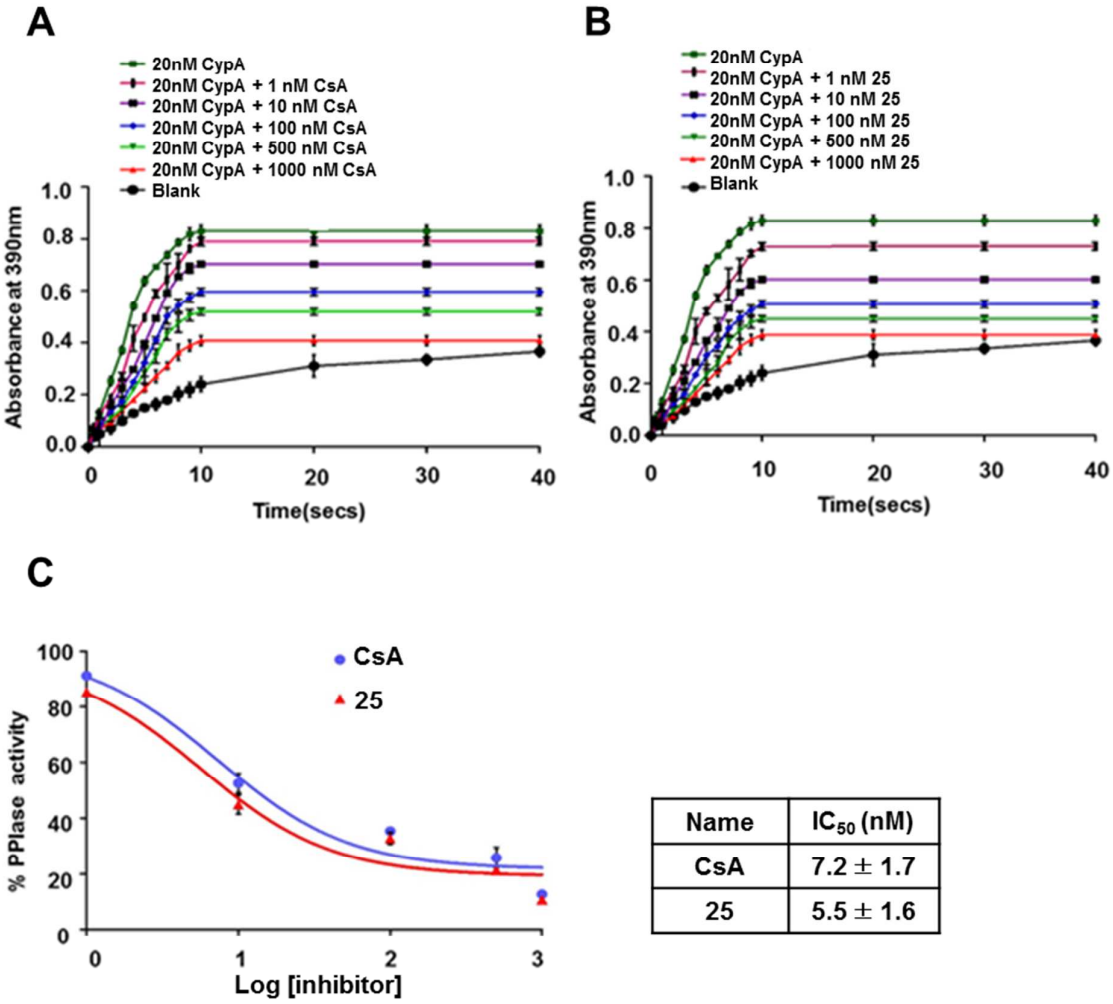

Name	IC_{50} (nM)
CsA	7.2 ± 1.7
25	5.5 ± 1.6

Figure S4. Dose response curve showing the inhibition of CypA enzymatic activity on treatment with CsA and **25**. The time course of the cis-to-trans isomerization of the Ala-Pro peptide bond in the substrate succinyl-Ala-Ala-Pro-Phe-4-nitroanilide is measured by the increase in A390 after the coupled hydrolysis by chymotrypsin. The uncatalyzed cis-trans isomerization in the absence of CypA is shown as a blank control, and isomerization catalyzed by 20 nM CypA and its inhibition with different concentations of (A) CsA or (B) **25** are shown as indicated. Data represent the mean ± S. D. (C) Dose response curve showing the inhibition of CypA enzymatic activity on treatment with different concentrations of CsA (●) or **25** (▲). IC_{50} value was calculated by non-linear regression using GraphPad Software. All data are representative of at least three different experiments and expressed as the mean ± S.D.

Lead 25 repressed interaction of CypA with viral non-structural proteins

Biochemical inhibiotry mechanism of **25** on HCV replication was investigated. The *in vitro* pull down assay showed that a CypA PPIase mutant (R55A) completely failed to bind to NS5A and NS5B, in contrast to wild type CypA (Figure S5A). **25** at 2 μM and 4 μM suppressed GST-CypA binding with NS5A or NS5B in a concentration-dependent manner (Figure S5B). Reversed experiments with GST-NS5A and GST-NS5B showed the same results (Figure S5C and D). Moreover, cell-based assays, such as co-immunoprecipitation (Figure S5E) and mammalian two-hybrid (Figure S5F)**,** confirmed the inhibitory effects of **25** on interactions between CypA and NS5A or NS5B. These observations indicate that the antiviral efficacy of **25** is achieved via suppression of CypA PPIase activity, similar to CsA.

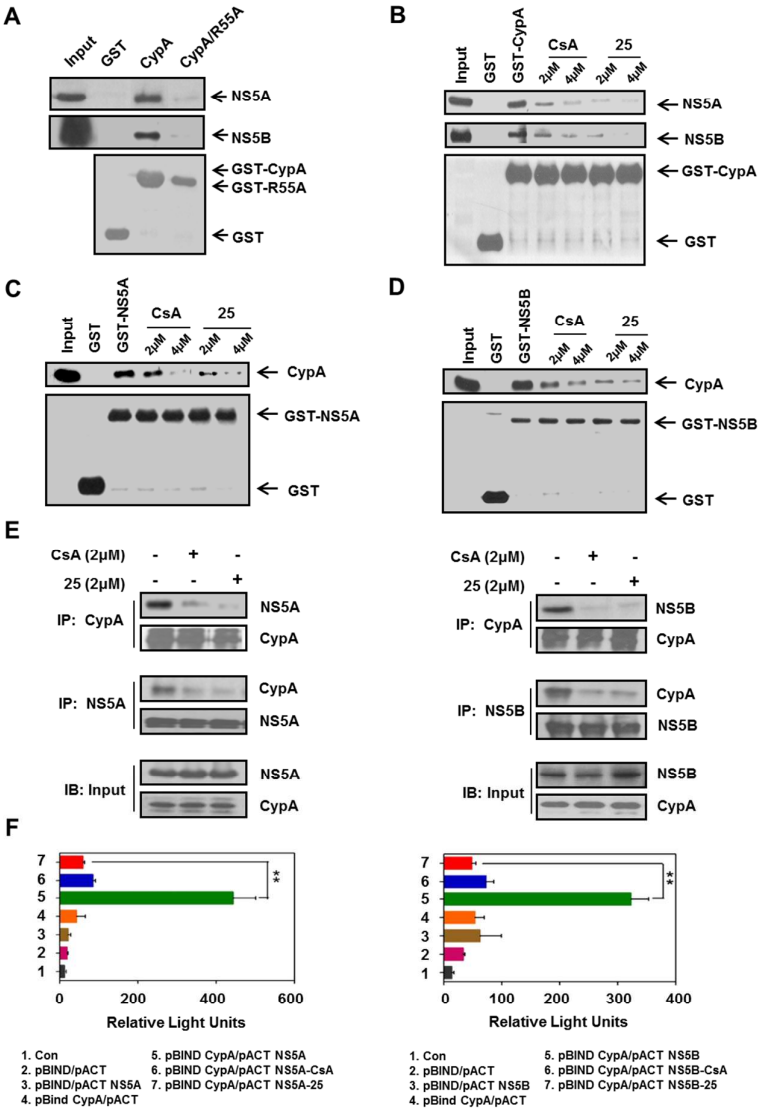

Figure S5. Disruption of the interaction between CypA and HCV non-structural viral proteins by **25**. (A) *In vitro* binding of CypA to NS5A or NS5B. Recombinant GST-CypA or GST-R55A CypA was incubated with thrombin-cleaved NS5A or NS5B and added to glutathione beads. Bound material was eluted and analyzed by Western blot. Wild type CypA efficiently bound to NS5A or NS5B. The CypA mutant R55A did not bind to viral proteins. (B-D) GST pulldown assay. Inhibition of protein-protein interactions was determined with increasing amounts of CsA or **25**. GST-fusion proteins were used as loading controls. All data are representative of at least three different experiments. (E) Co-immunoprecipitation assay of CypA with NS5A (left) or NS5B (right) in HCV replicon cells in the presence or absence of CsA or **25**. Western blot analysis was conducted using antibodies. Input, cell lysates. All data are representative of at least three different experiments. (F) Mammalian two-hybrid assay for analysis of CypA binding to HCV NS5A (left) or NS5B (right) proteins. Data represent the mean ± S. D.; n = 3. $^{**}p < 0.01$ versus untreated cells.

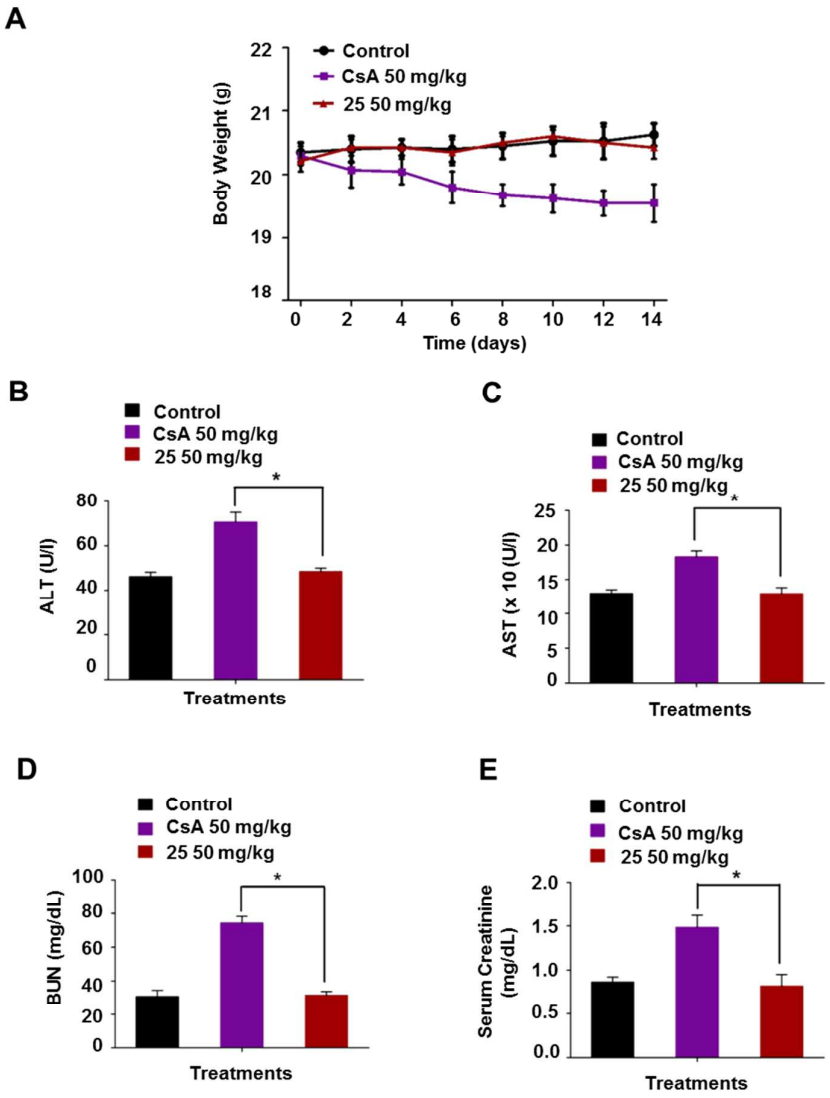

Figure S6. Effect of **25** on liver and kidney toxicities. A total of 15 BALB/c mice were divided into three groups (each n = 5) and were used as untreated (control) and two treated groups (50 mg/kg of CsA, or **25**) for 2 weeks. (A) Changes in body weight during the experiment. Data represent mean ± S.D.; n = 3 (B and C) Serum levels of ALT, and AST were measured after systemic administration of CsA or **25**. CsA treated group showed elevation in ALT and AST enzyme levels. Data represent mean ± S.D.; n = 3. * $p< 0.05$ versus CsA. (D and E) The serum levels of BUN and creatinine levels were increased in the CsA treated group as compared to untreated and **25**. Data are expressed as mean ± S.D.; n = 3. * $p< 0.05$; versus CsA for BUN or creatinine levels.

Chemistry

*2-[(4-Bromophenyl)-(2-1H-indol-3-ylacetyl)amino]-N-cyclohexyl-2-(2,3,4-trimethoxyphenyl)acetamide (**26**)*. The procedures applied to the synthesis of **5** were used with cyclohexyl isocyanide **1a** (55 mg, 0.50 mmol), 2,3,4-trimethoxybenzalde hyde **2e** (100 mg, 0.51 mmol), 4-bromoaniline **3a** (108 mg, 0.63 mmol), 3-indoleacetic acid **4b** (88 mg, 0.50 mmol), and 2,2,2-trifluoroethanol at rt to obtain bis-amide **26** as a white solid (163 mg, 50%). Mp: 143.2–146.5 °C. IR (cm $^{-1}$): 3308, 1644. ^{1}H NMR (300 MHz, $CDCl_3$) δ: 8.00 (s, 1H), 7.37–7.29 (m, 4H), 7.24–7.19 (m, 2H), 7.16–7.11 (m, 1H), 7.07–7.00 (m, 2H), 6.63 (d, *J* = 8.7 Hz, 1H), 6.37–6.34 (m, 2H), 5.51 (d, *J* = 8.4 Hz, 1H), 3.83–3.75 (m, 1 H), 3.82 (s, 3H), 3.77 (s, 3H), 3.76 (s, 3H), 3.56 (s, 2H), 1.92–1.82 (m, 2H), 1.68–1.54 (m, 3H), 1.38–1.23 (m, 2 H), 1.14–0.91 (m, 3H). ^{13}C NMR (125 MHz, $CDCl_3$) δ: 171.5, 169.1, 154.0, 152.2, 141.3, 139.1, 135.9, 132.0, 131. 5, 127.1, 125.6, 123.0, 121.9, 121.8, 120.0, 119.3, 118.7, 110.9, 109.2, 106.5, 61.0, 60.5, 58.5, 55.8, 48.7, 32.7, 32.0, 25.4, 24.8, 24.7. MS (ESI): *m/z* 656 $(M+Na)^+$. Anal. calcd for $C_{33}H_{36}BrN_3O_5$: C, 62.46; H, 5.72; N, 6.62. Found C, 62.27; H, 5.69; N, 7.01. HPLC: purity 97.3%.

Bioloical Tests

Materials and methods

Antibodies. Antibodies specific to CypA, glutathione S-transferase (GST), HCV NS5A, STAT1, STAT2, IRF9, OAS1 and ISG15 were purchased from Santa Cruz Biotechnology (Santa Cruz, CA). Antibodies against HCV NS5B and NFAT1 were purchased from Enzo Life Sciences (Plymouth Meeting, PA) and Abcam (Cambridge, MA), respectively.

Compounds. Cyclosporin (CsA) was purchased from Sigma (St. Louis, MO). Bis-amides were synthesized and stored at 5 mM concentration in dimethyl sulfoxide (DMSO) as a stock solution. Recombinant human IFN-α 2A and ribavirin were purchased from Sigma (St. Louis, MO) and stored at -20 °C. Telaprevir was obtained from Selleck Chemicals (Houston, TX).

Cell culture. Human hepatoma Huh7 cells were cultured in Dulbecco's modified Eagle's medium supplemented with 10% heat-inactivated fetal bovine serum (FBS), 100 units/mL of penicillin, 100 μg/mL of streptomycin, 1% L-glutamine, and 1x nonessential amino acid (NEAA) mixture. Huh7 cells with the subgenomic HCV genotype 1b (Con1/SG- Neo(I) hRluc FMDV2aUb) were provided by Prof. Charles Rice (The Rockefeller University and Apath, LLC, St. Louis, MO). Huh7 cells with the full length genotype 2a JFH1 were cultivated by Prof. Marc P. Windisch (Institute Pasteur, Korea). All Huh7-derived replicon cells were propagated in DMEM with 10% FBS, 100 units/mL of penicillin, 100 μg/mL of streptomycin, and 1x NEAA mixture and selected using 0.5 mg/mL G418 from Duchefa Biochemie (Amsterdam, The Netherlands).

Peptidyl-prolyl *cis-trans* isomerase (PPIase) activity. PPIase activity of CypA was determined in presence or absence of inhibitors by the method as previously described[2, 3] using Succ-Ala-Leu-Pro-Phe-p-nitroaniline (Sigma, St. Louis, MO) as a substrate. All the reagents were pre-equilibrated at 0 °C. The final reaction mixture (1 mL) contained 20 nM of CypA, 4 mM of substrate and 100 μg of α-chymotrypsin (Sigma, St. Louis, MO) and assay buffer (50 mM HEPES, 100 mM NaCl, pH 8.0 at 0 °C). Reaction was performed at 4 °C and the changes in the absorbance were monitored at 390 nm for 3 min on a UV-vis spectrophotometer (*Pharmacia Biotech,* Massachusetts USA). PPIase activity was calculated from the absorbance data. PPIase activity (%) = (Abs390 [Inhibitor] – Abs390 blank)/ (Abs390 No Inhibitor – Abs390 blank). IC_{50} was calculated from the PPIase activity curve by non-linear regression using GraphPad Software.[4]

Isothermal titration calorimetry. ITC experiments were performed using a Microcal 200 isothermal titration microcalorimeter (Microcal, Inc., Northampton, MA) as described by Kim et al.[5] In briefly, typical titrations involved injecting 1.5 μL 1.25 mM of **25** in 40% EtOH, 10 mM Tris pH 7.0 into the sample cell (filled with 0.06 mM CypA-GST fusion protein in 40% EtOH, 10 mM Tris pH 7.0). The syringe stir rate was set to 500 rpm. The data fitting was performed using Origin software (version 7.0) and the fitting process was iterated until getting the best fit determined by the chi-square minimization method. Fitting the binding isotherms in this way provided data on the binding constant (Ka), change in enthalpy (ΔH), and stoichiometry of binding (n). The binding Gibbs free energy (ΔG) was calculated from the enthalpy change (ΔH) and binding constant (Ka) using the equation: $\Delta G = RT\ln Ka = \Delta H - T\Delta S$, where R is the gas constant and T is the absolute temperature in degrees Kelvin. Meanwhile, the stoichiometries (n) of the different interactions were determined from Two Sets of Site models.

Luciferase assay. HCV Replication in Con1b replicon cells was determined by monitoring *Renilla* luciferase activity (Promega, Madison, WI). The *Renilla* luciferase activity reflected the amount of HCV RNA synthesized. The Relative luciferase activity obtained from CsA or **25** treated cells were normalized to the corresponding values obtained with untreated cells.

Expression and purification of GST-fusion and recombinant proteins. The pGEX-KG plasmid was used to express recombinant proteins in *E. coli*. Full length GST-CypA, mutant GST-CypAR55A (mutation at the PPIase site), GST-CypB, GST-NS5A and GST-NS5B were generated using standard cloning procedures. The pGEX-KG bacterial expression vector was transformed into TOP10F cells (Promega, Madison, WI). Bacterial cultures were grown in LB medium with 100 μg/mL ampicillin until an optical density of 0.8-1.0 at 600 nm was reached. Thereafter, GST fusion protein expression was induced by adding 0.1 mM isopropyl-beta-D-thiogalactopyranoside, and incubation was continued for 4 more h at 30 °C. The bacteria were then pelleted at 4 °C for 20 min at 340*g* and resuspended in 10 mL PBST (PBS containing 1% Triton X-100) and sonicated by adding 1 mM PMSF at a 25% amplitude for 30 min. After sonication, bacterial extracts were centrifuged at 340*g* for 15 min at 4 °C and supernatants containing the GST proteins were stored at -80 °C. GST-fusion proteins were cleaved overnight in thrombin cleavage buffer containing 50 units of thrombin to release recombinant proteins from GST-bound glutathione resin. Supernatants containing the recombinant protein were collected and used for pull-down assays.

GST pull-down assay. Recombinant proteins GST-CypA, GST-NS5A or GST-NS5B were produced by affinity purification. Approximately 100 μg of GST protein or GST-CypA fusion protein were incubated with 50 μL of glutathione-agarose beads at 4 °C for 4 h with rotation. After washing with PBST buffer (phosphate buffer saline containing 1% Triton X-100), GST-bound resins were incubated with 10 μg of thrombin-cleaved full-length NS5A or NS5B protein in 500 μL binding buffer (20 mM Tris-HCl pH 7.9, 0.5 M NaCl, 10% glycerol, 10 mM DTT and 1% NP-40) at 4 °C overnight with rotation. In a similar fashion, thrombin-cleaved CypA protein was incubated with purified GST-NS5A or GST-NS5B and binding was assessed. Proteins bound to glutathione-agarose beads were eluted with 25 μL 5x SDS-PAGE buffer, heated for 5 min and analyzed by Western blot using anti-GST, anti-CypA, anti-NS5A and anti-NS5B antibodies.

Co-immunoprecipitation. For co-immunoprecipiation, 4 μg of specific antibody and 1 mg/mL of HCV Con1b replicon protein lysate were rotated for 4 h at 4 °C in a total volume of 500 μL PBS. Then, 20 μL of washed protein A/G PLUS agarose (Santa Cruz, CA) was added and incubated overnight at 4 °C. Samples were washed three times with Triton wash buffer, resuspended and denatured in 5x SDS-PAGE buffer for 5 min at 95 °C and subjected to Western blot analysis.

Mammalian two-hybrid system. To evaluate intracellular CypA-NS5A and CypA-NS5B interactions, two-hybrid screening technology was used according to the manufacturer's instructions using the checkmate mammalian two-hybrid system (Promega, Madison, WI). Briefly, pACT- and pBIND-based plasmids were co-transfected (TurboFect, FermentasC) with the pGL5*luc* reporter construct into Huh7 cells and incubated at 37 °C. After 72 h, cell lysates were assessed for luciferase activity.

Isolation of splenocytes from mice. Female BALB/c mice (7-8 weeks old) were obtained from Orient Bio, Inc. (Sungnam, Korea). Animals were maintained in a pathogen-free environment and allowed to acclimatize before experimentation. Mice were sacrificed by cervical dislocation and spleens were removed into a petri dish containing RPMI supplemented with 10% FBS, 100 units/mL of penicillin, and 100 μg/mL of streptomycin. Spleens were dispersed through a nylon mesh to generate a single cell suspension followed by depletion of RBC by using RBC lysis buffer (Sigma, St. Louis, MO). Splenocytes were washed and cultured in RPMI complete medium.

Toxicity assay in BALB/c mice. A total of 15 6-week-old female BALB/c mice were used to assess the toxicity of **25** or CsA. The animals were divided into three groups (n = 5), with one group as an untreated control. A group of five mice were injected intraperitoneally with CsA or **25** at a daily dose of 50 mg/kg body weight. After 14 days post-injection, blood samples were collected from the treated and control groups. Body weights were obtained to assess systemic toxicity in mice. To assess hepatotoxicity, AST and ALT activities were measured using a GOT·GPT kit (Asan Pharm, Korea) according to the manufacturer's protocol adjusted to 96-well microplates. Results from these assays are presented as AST and ALT activity in IU/L units. For nephrotoxicity, blood urea nitrogen (BUN) levels in the serum were measured using a BUN enzymatic kit (Bioo Scientific, Austin, TX) and serum creatinine levels were measured using a mouse creatinine kit (Crystal Chem, Inc., Downers Grove, IL).

Immunofluorescence. HCV replicon cells were seeded on coverslips in 12-well plates to ~70% confluence per well for 24 h. For fixation, cells were washed three times with PBS and fixed in a 4% paraformaldehyde solution for 20 min at room temperature. Cells were again washed three times with PBS. For permeabilization, cells were incubated for 15 min with 0.5% Triton X-100 in PBS and washed three times with PBS prior to incubation with the primary antibody. The primary antibody was diluted to the desired concentration, typically 1:100, in 1x PBS buffer containing 3% bovine serum albumin (BSA) to prevent nonspecific binding. After overnight incubation, cells were washed three times with PBS and incubated in the dark with anti-rabbit or anti-mouse IgG secondary antibodies conjugated with Alexa 488 or Alexa 546 (Invitrogen, CA) diluted 1:250 in PBS with 3% BSA for 2 h. Cells were counterstained with DAPI (4′,6′-diamidino-2-phenylindole) and mounted on glass slides (Vector Mount, CA). Photographs of prepared samples were taken using a Zeiss confocal microscope (Zeiss, Germany).

Statistical analysis. Data analysis was performed using 2-tailed student's t-test. Data are expressed as the mean ± standard deviation (s.d.) of at least three independent experiments.

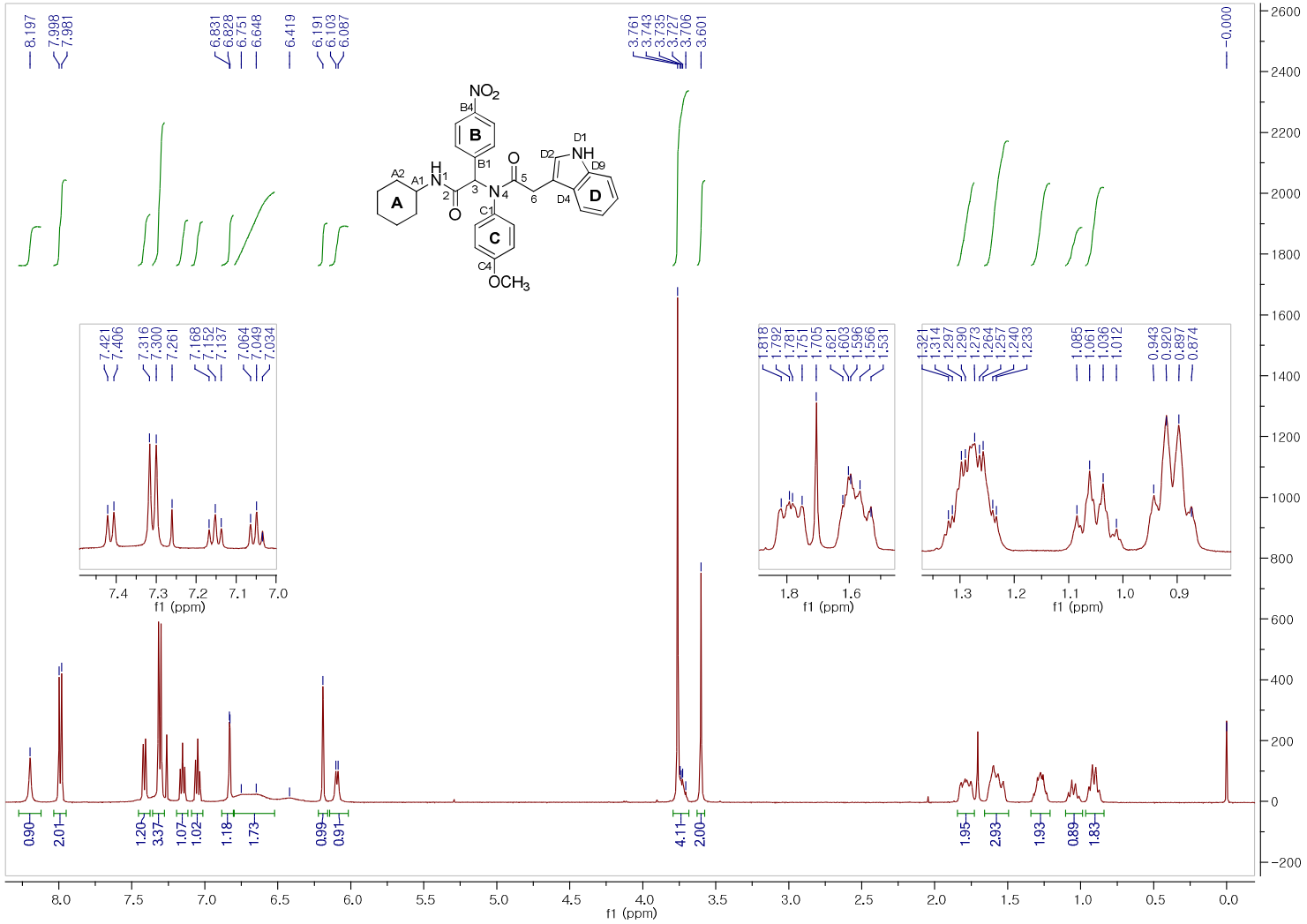

Figure S7. ^{1}H NMR (500 MHz, $CDCl_3$) spectrum of **7**.

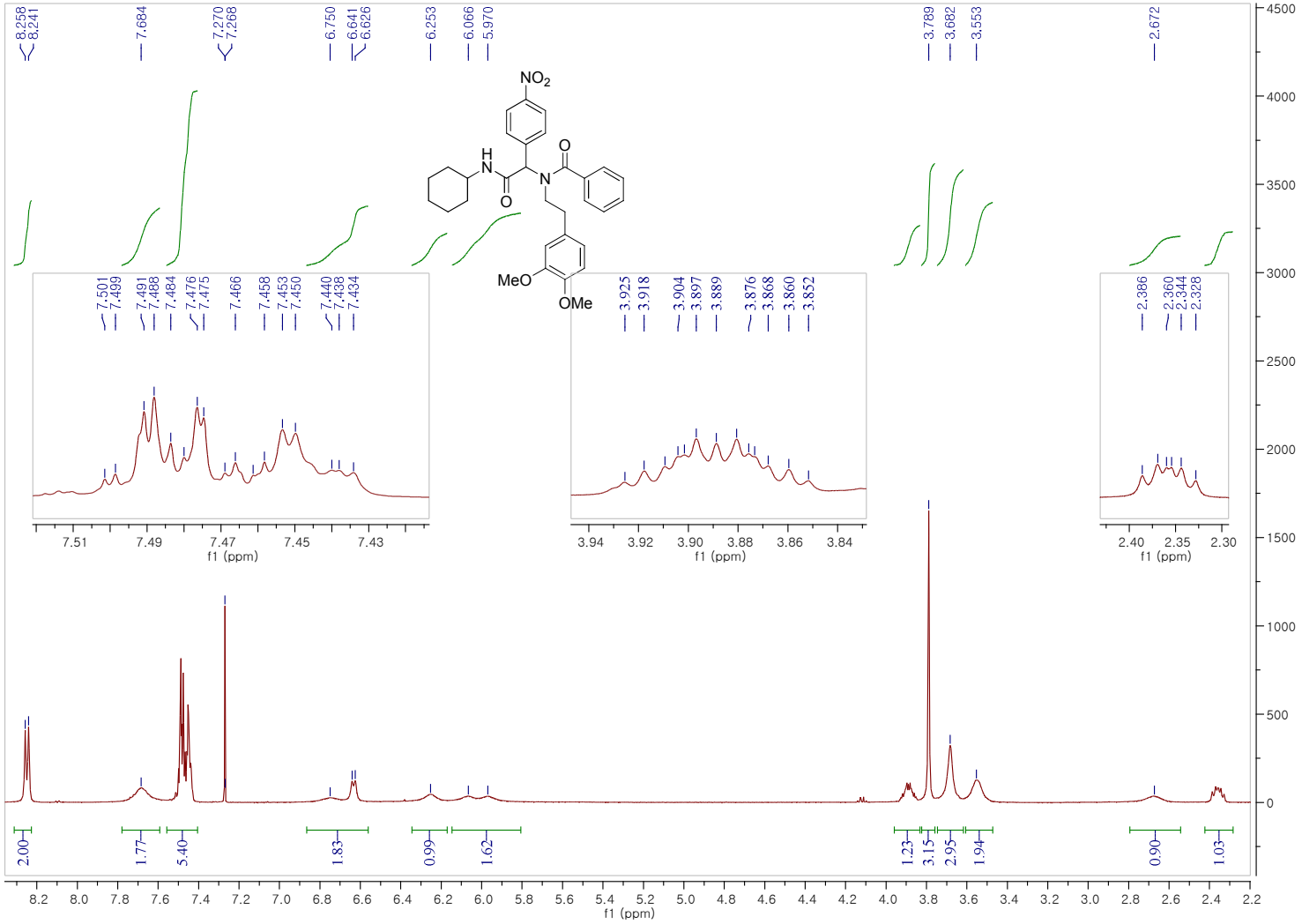

Figure S8. ^{1}H NMR (500 MHz, $CDCl_3$) spectrum of **23** (8.3–2.2 ppm).

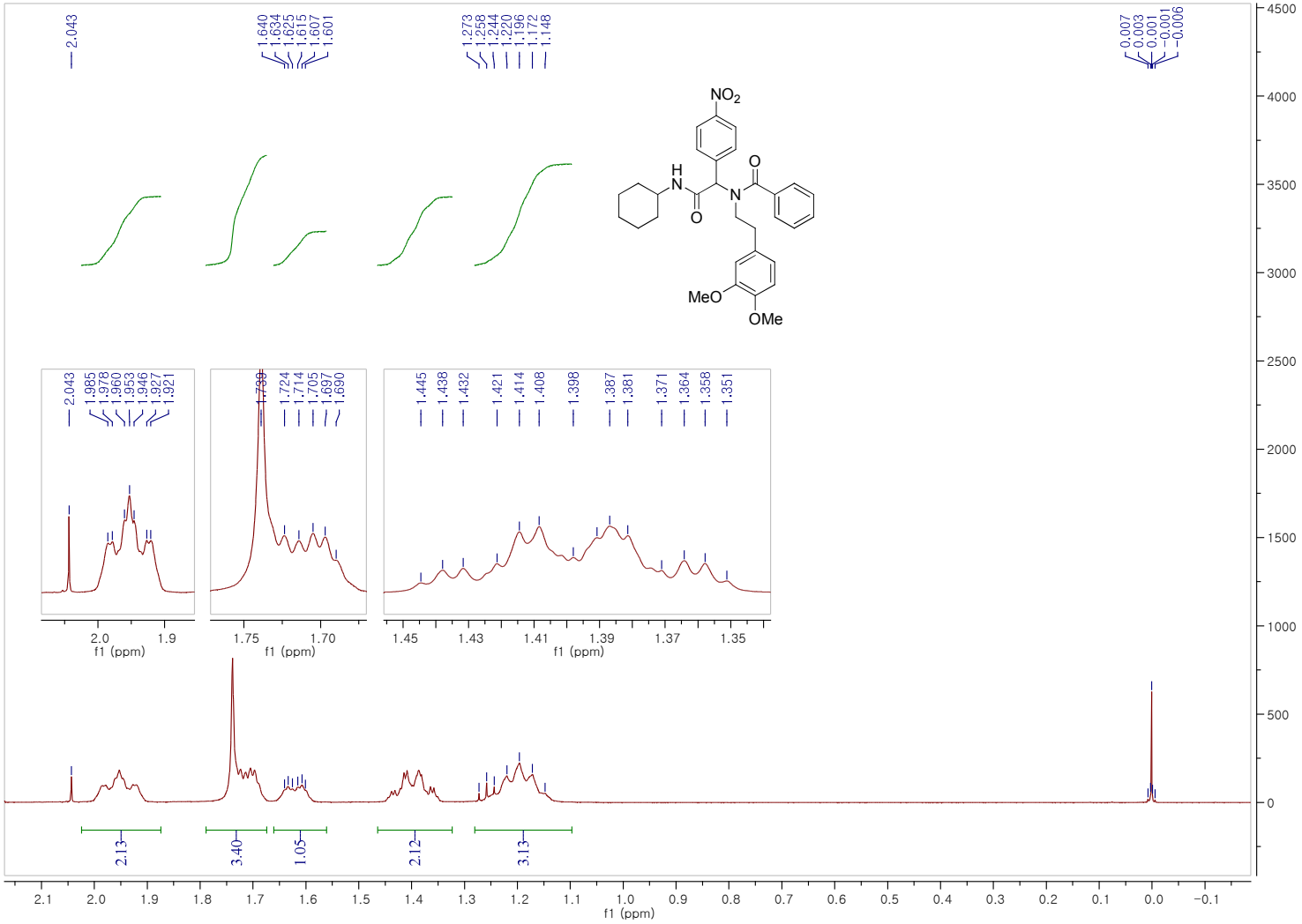

Figure S9. ^{1}H NMR (500 MHz, $CDCl_3$) spectrum of **23** (2.1–0.0 ppm).

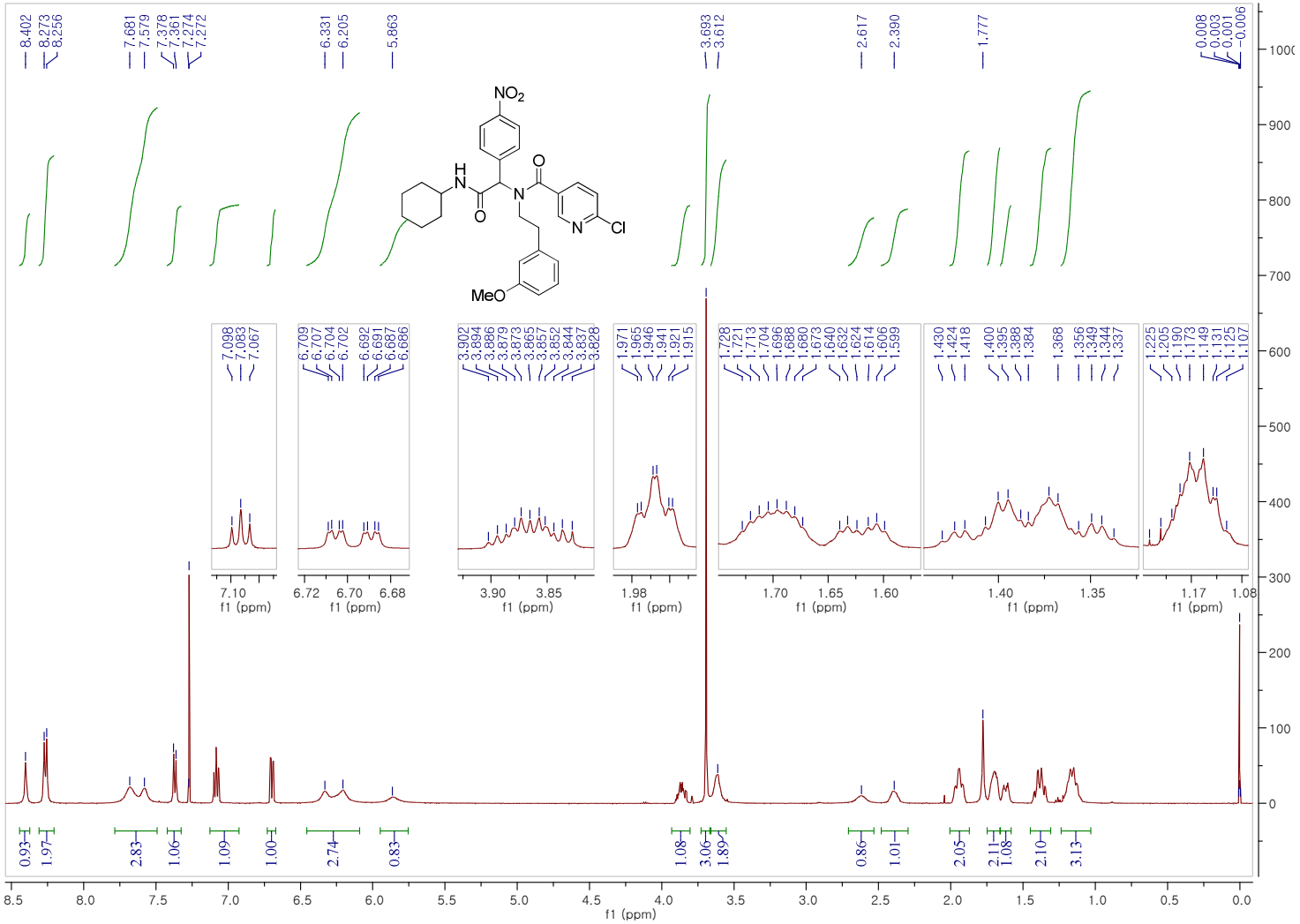

Figure S10. ^{1}H NMR (500 MHz, $CDCl_3$) spectrum of **24**.

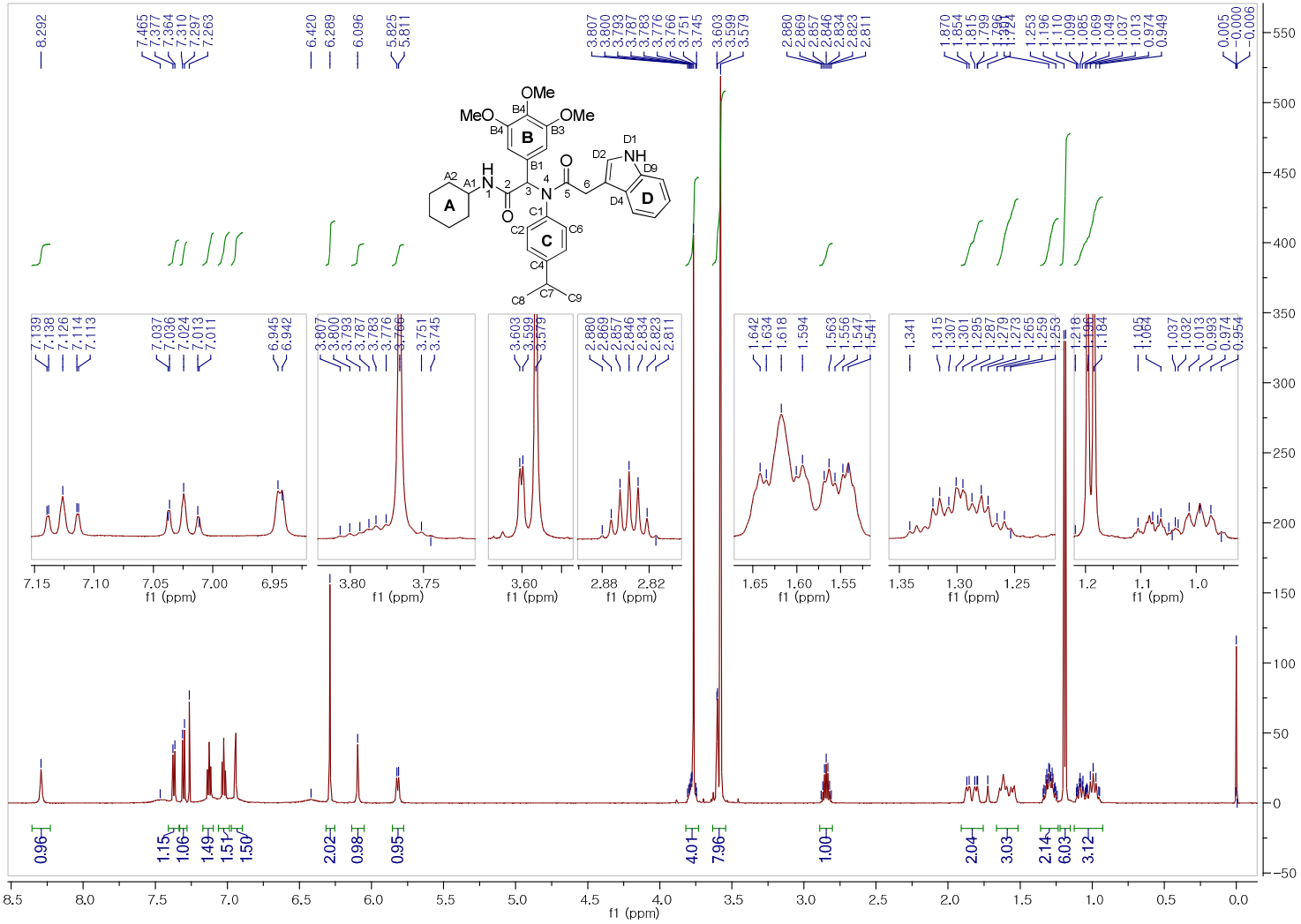

Figure S11. ^{1}H NMR (600 MHz, $CDCl_3$) spectrum of **25**.

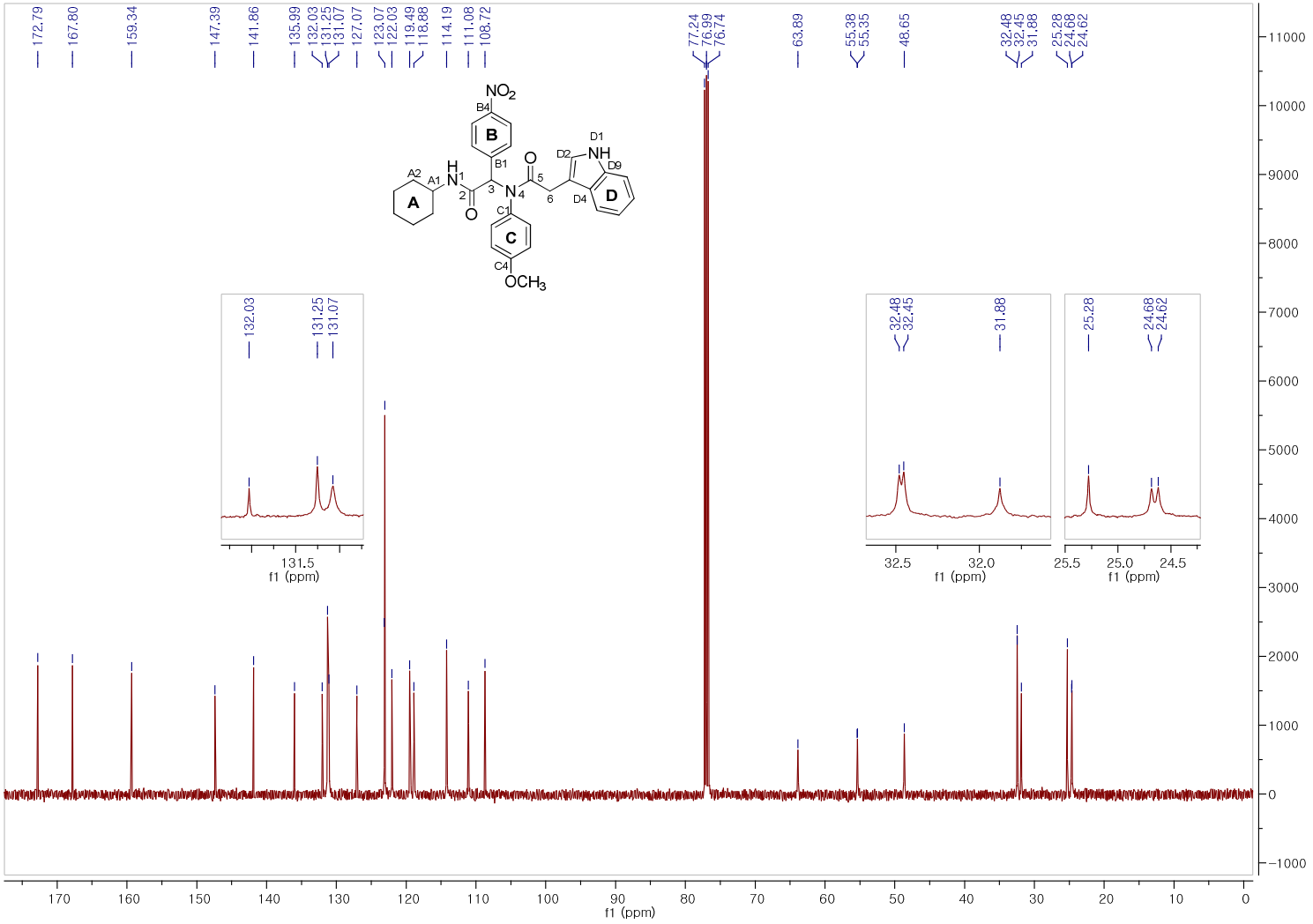

Figure S12. ^{13}C NMR (125 MHz, $CDCl_3$) spectrum of **7**.

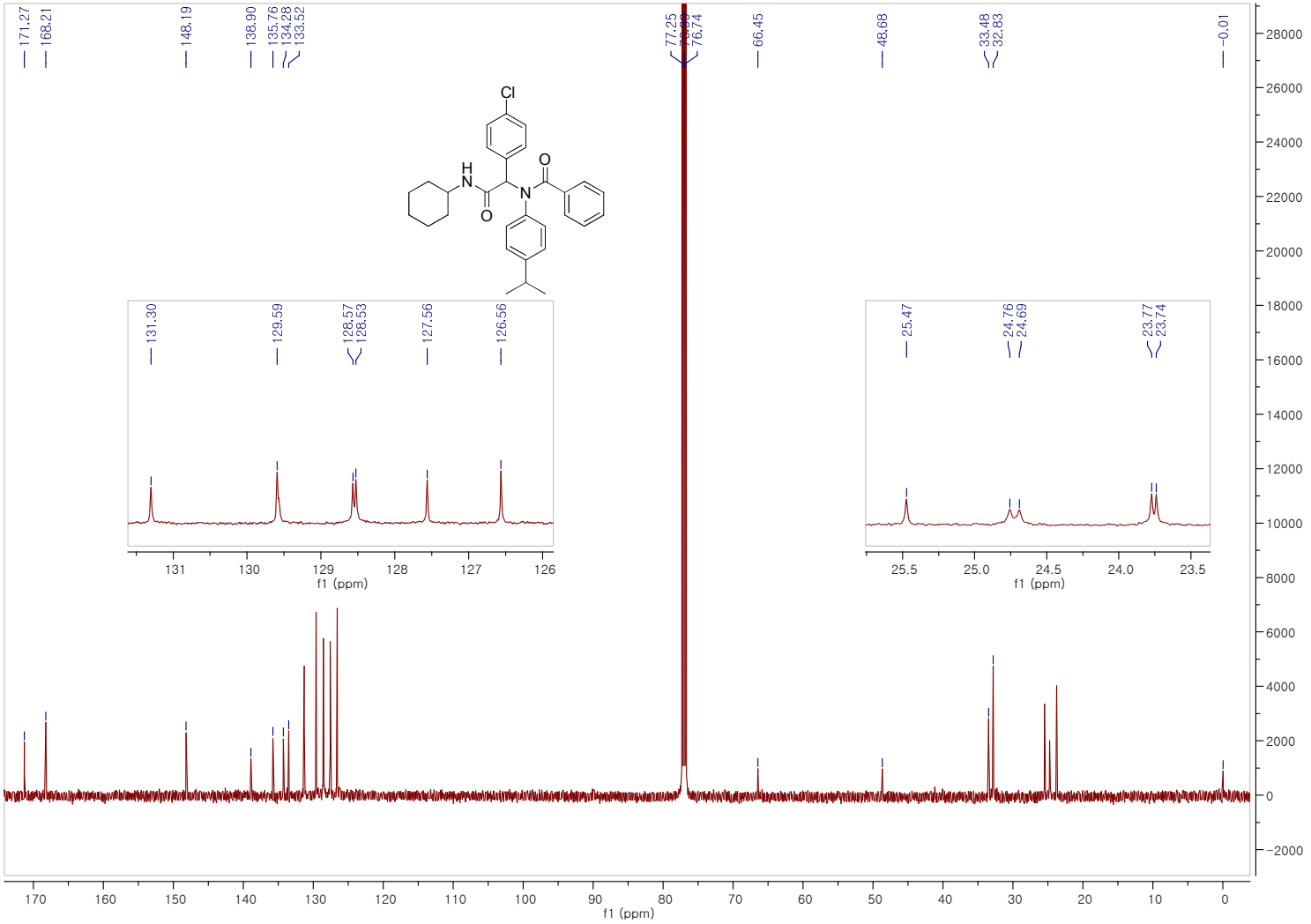

Figure S13. ^{13}C NMR (125 MHz, $CDCl_3$) spectrum of **20**.

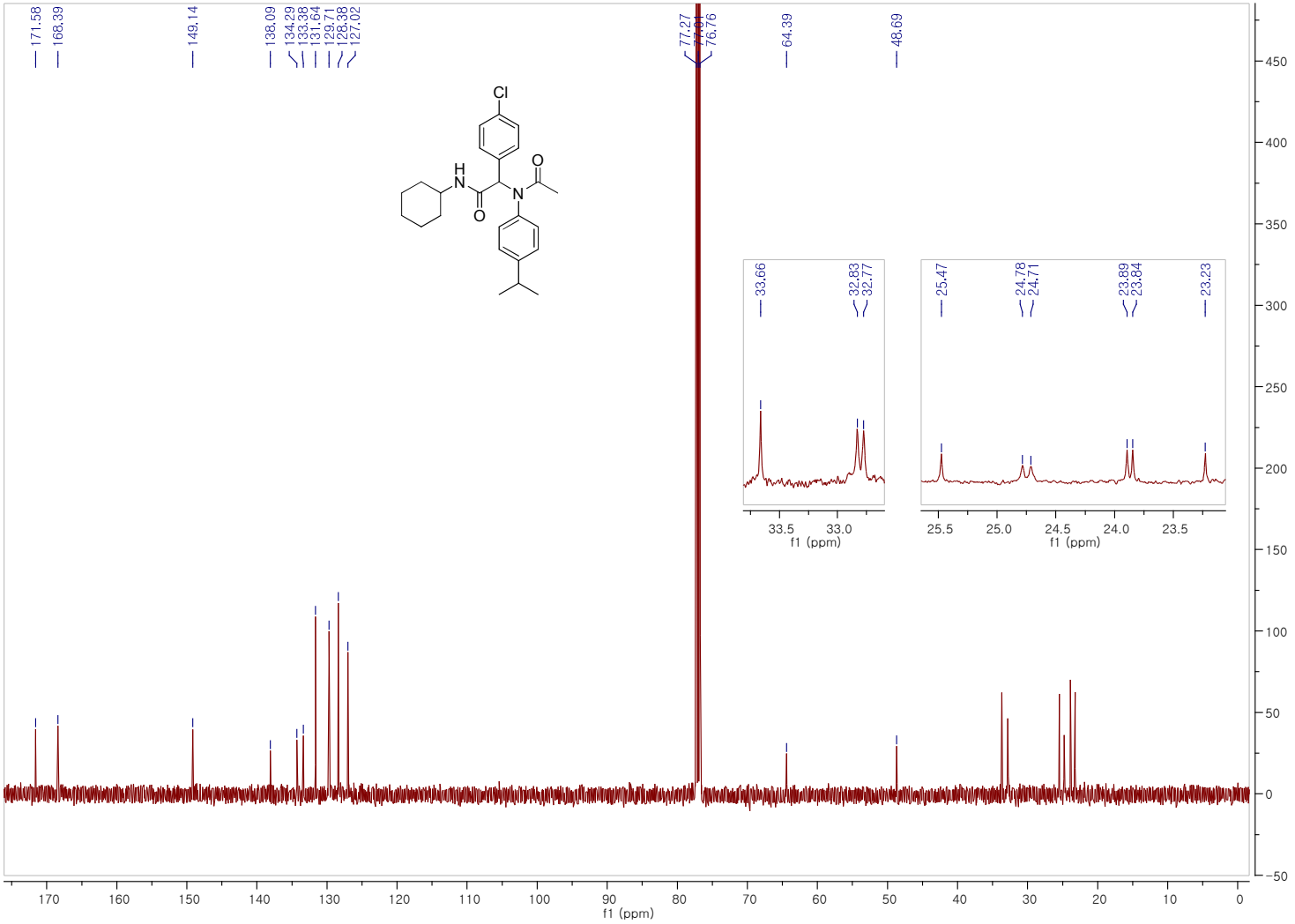

Figure S14. ^{13}C NMR (125 MHz, $CDCl_3$) spectrum of **21**.

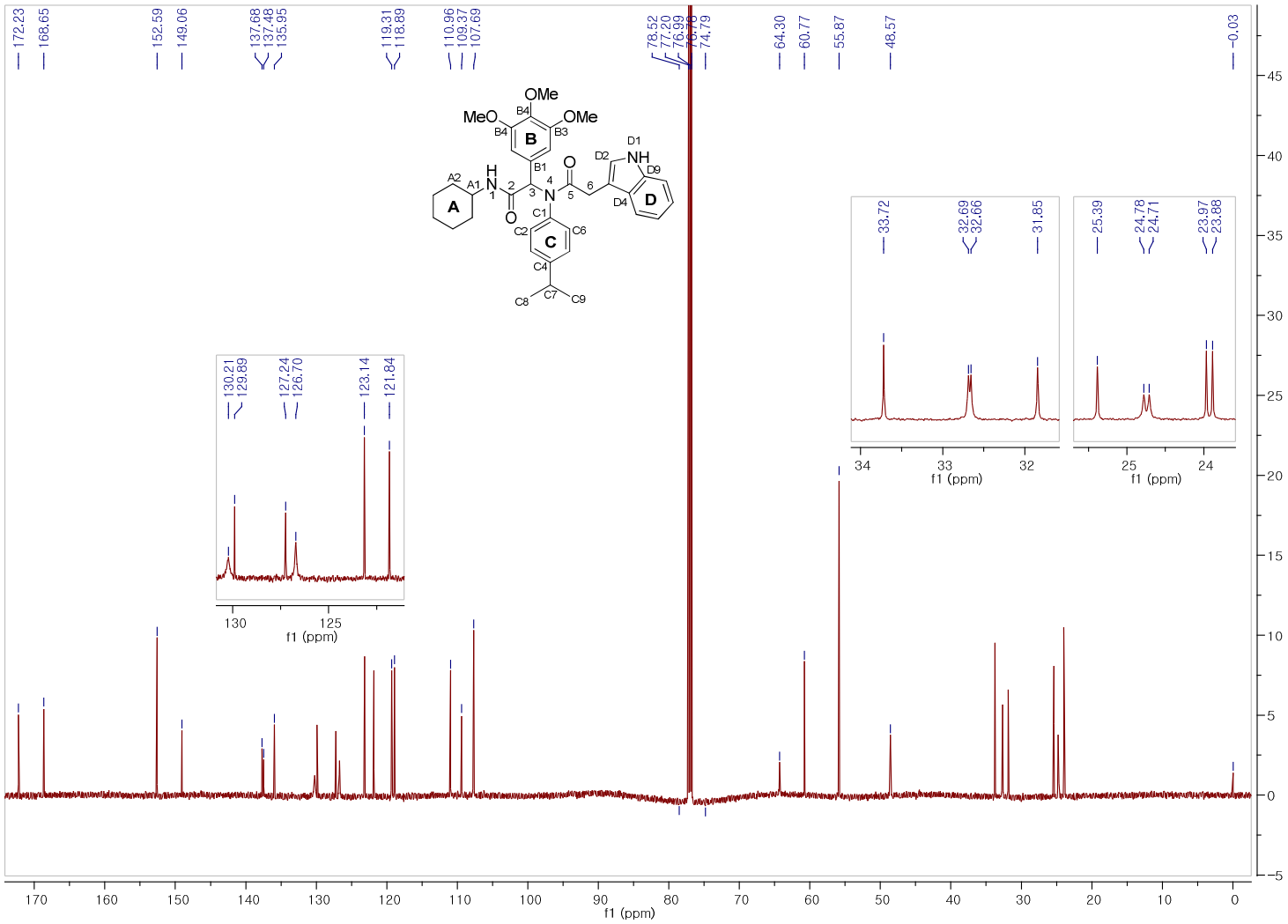

Figure S15. ^{13}C NMR (150 MHz, $CDCl_3$) spectrum of **25**.

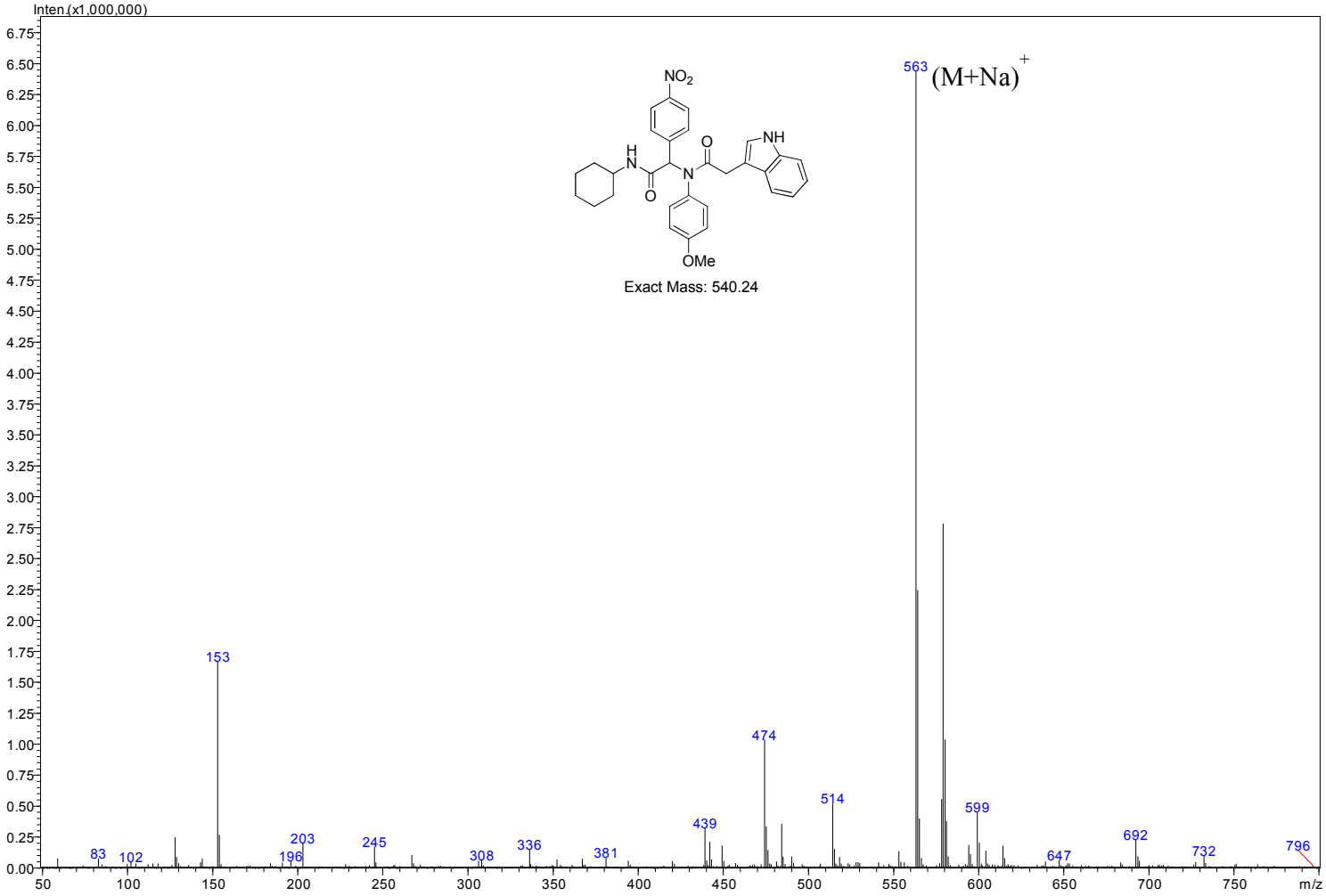

Figure S16. Mass spectrum of **7**.

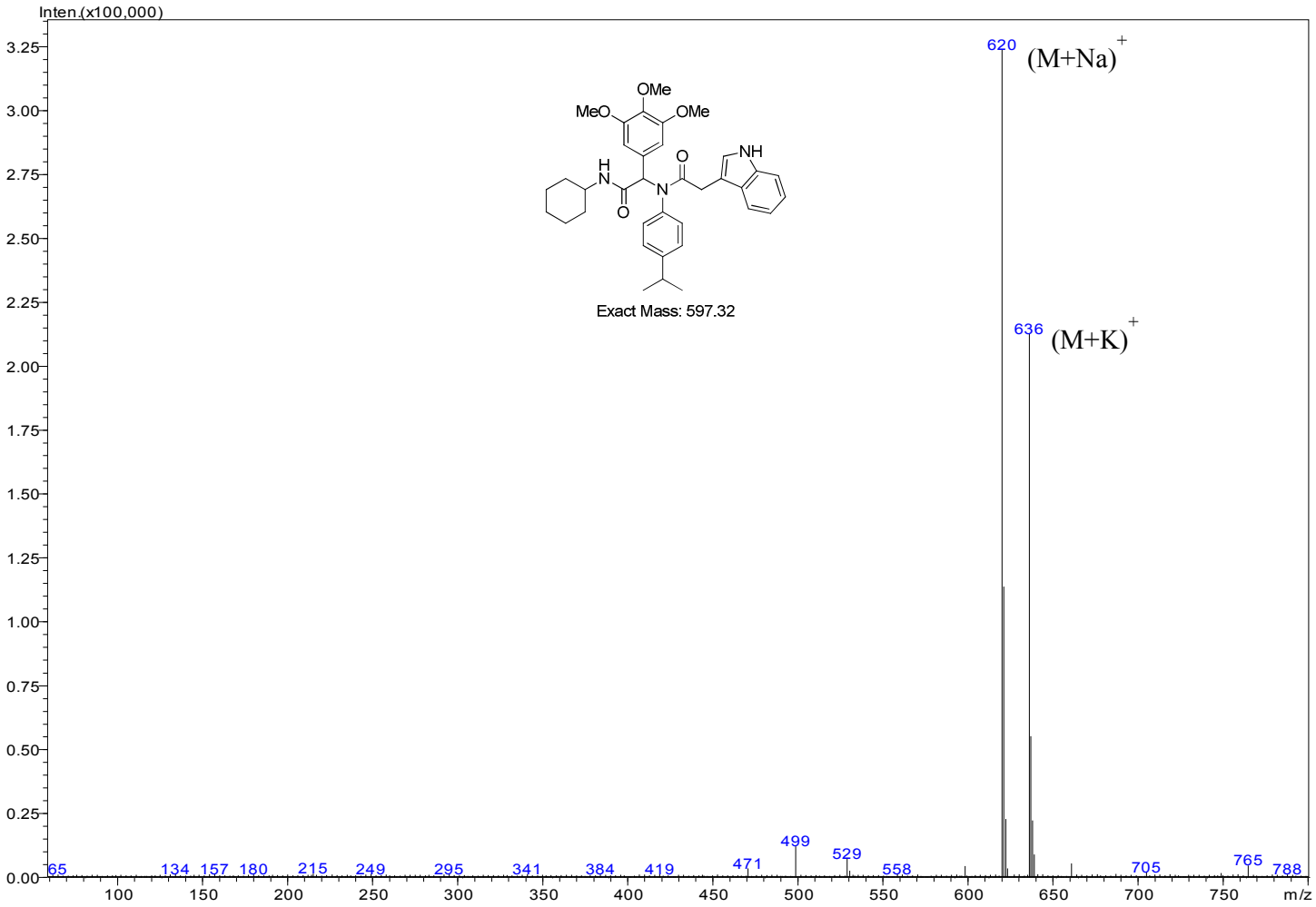

Figure S17. Mass spectrum of **25**.

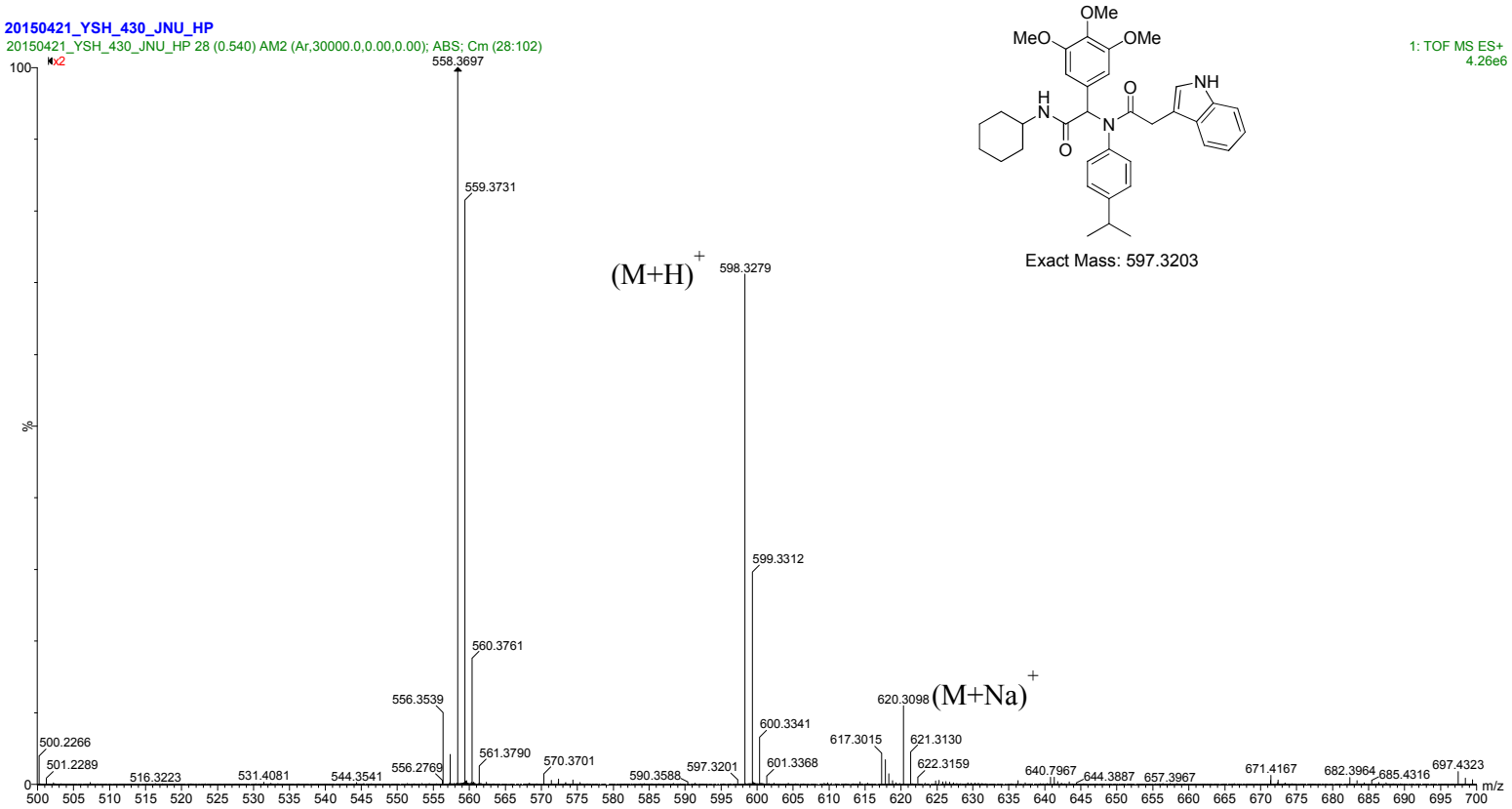

Figure S18. HRMS spectrum of **25**.

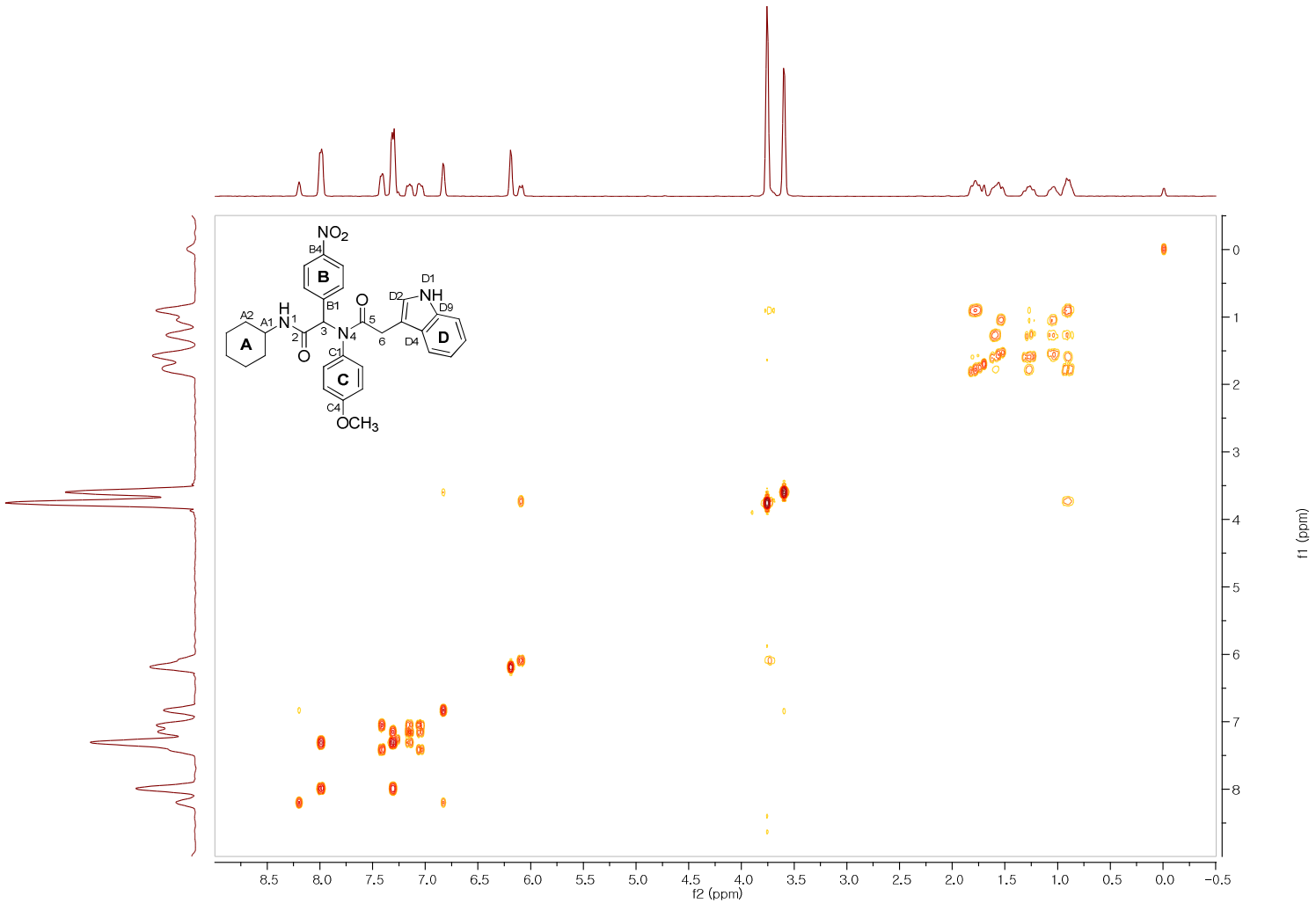

Figure S19. ^{1}H-^{1}H COSY (500, 500 MHz, $CDCl_3$) spectrum of **7**.

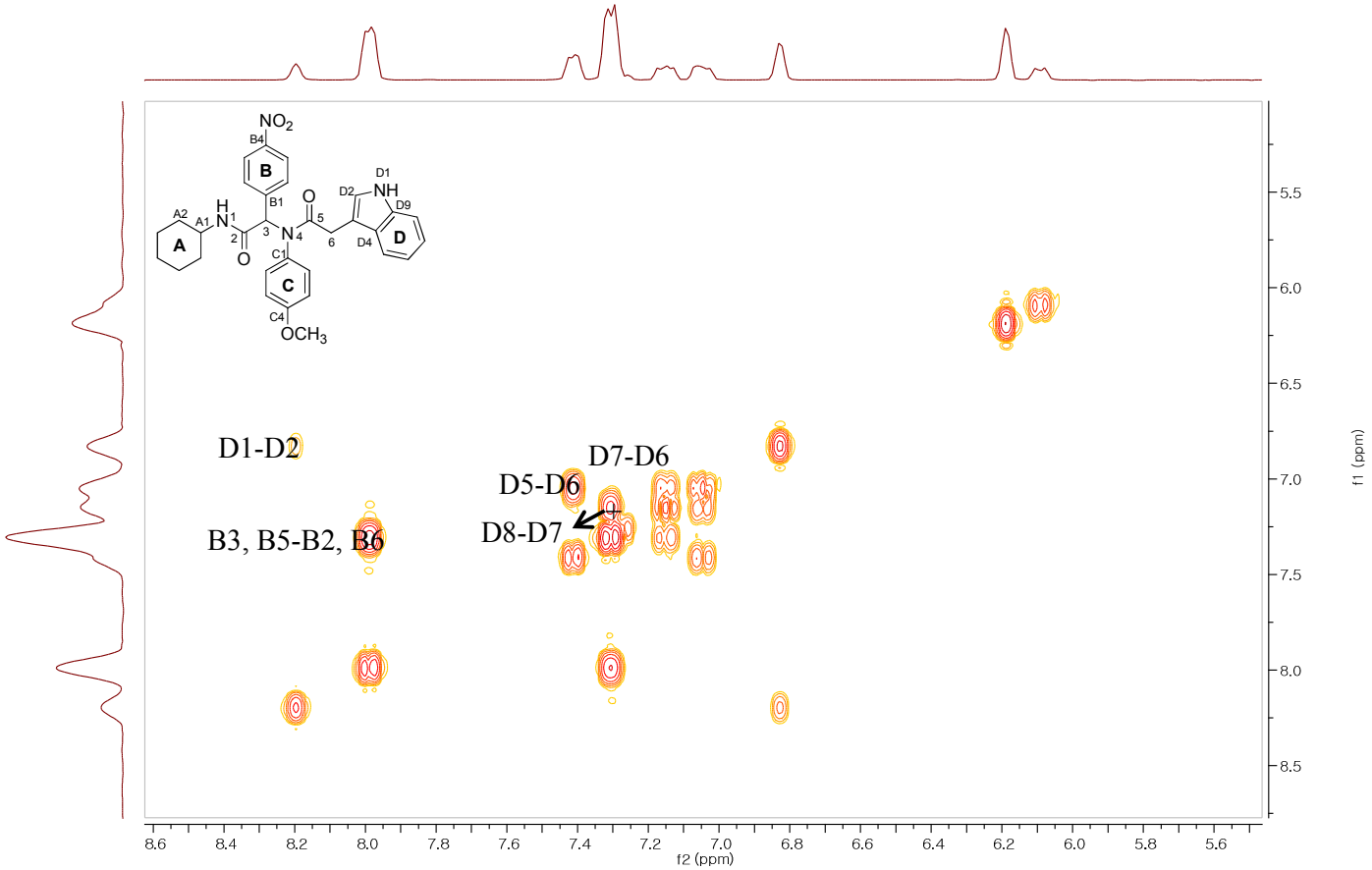

Figure S20. ^{1}H-^{1}H COSY (500, 500 MHz, $CDCl_3$) spectrum of **7** (8.6–5.6 ppm).

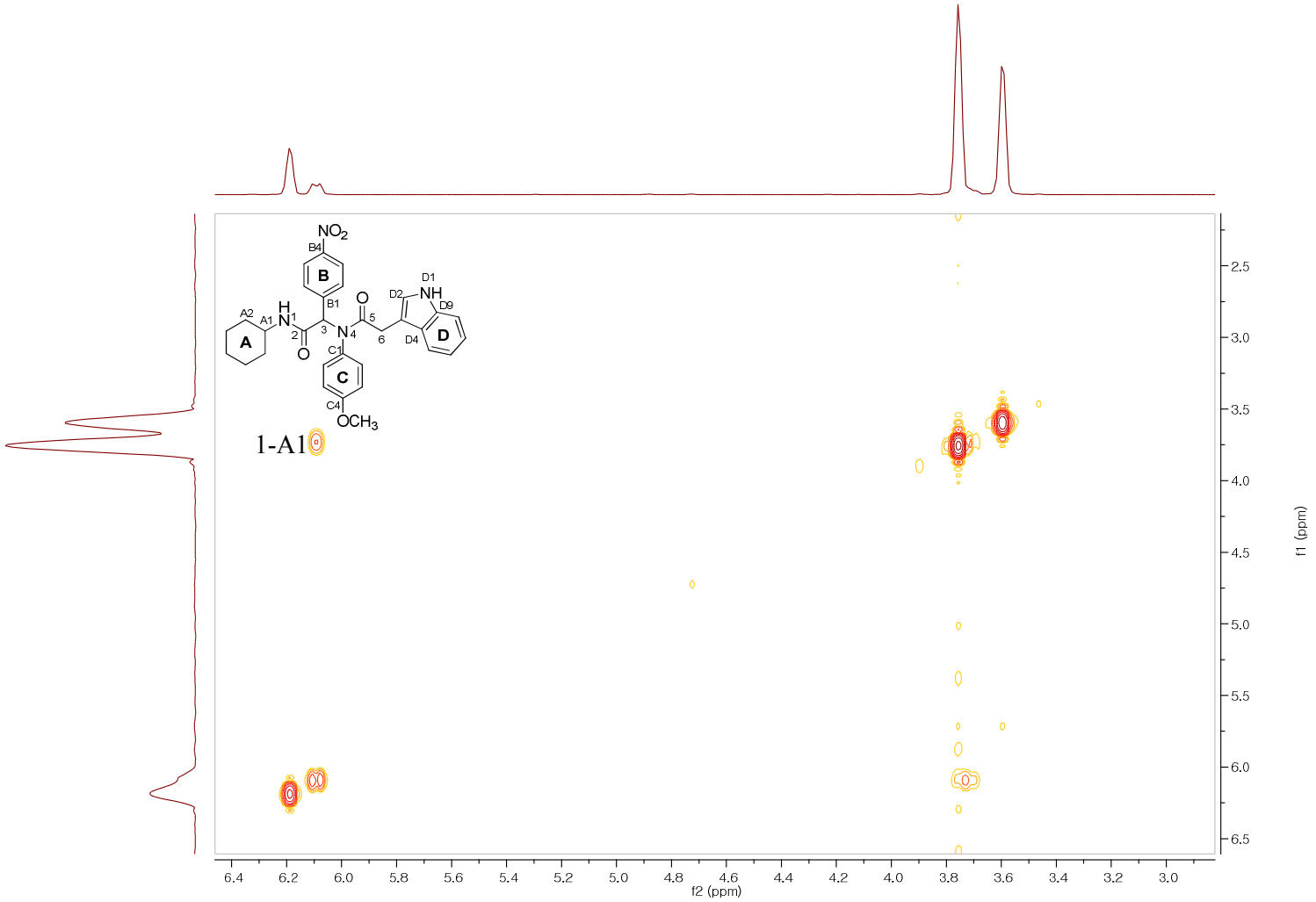

Figure S21. ^{1}H-^{1}H COSY (500, 500 MHz, $CDCl_3$) spectrum of **7** (6.4–3.0 ppm).

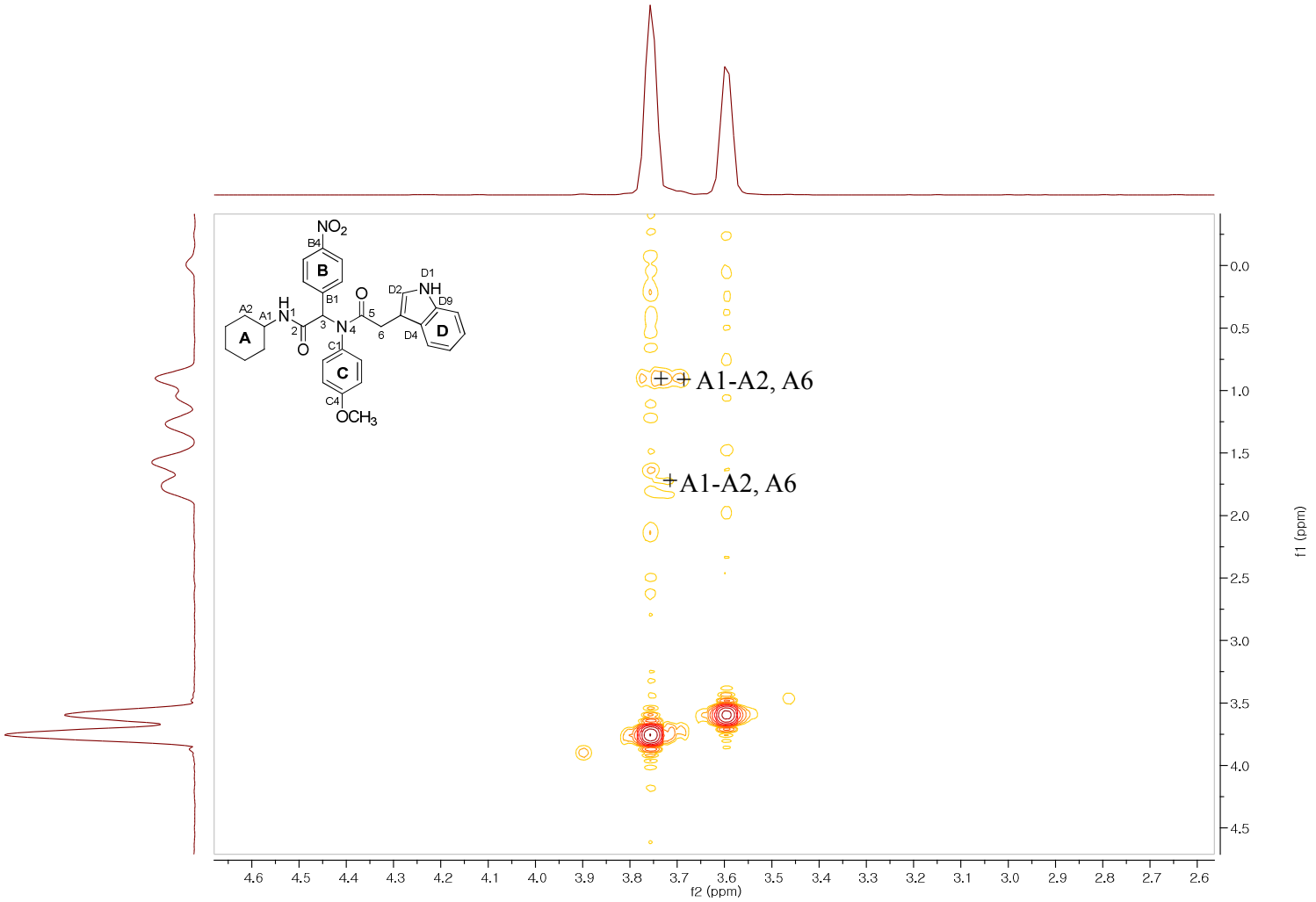

Figure S22. ^{1}H-^{1}H COSY (500, 500 MHz, $CDCl_3$) spectrum of **7** (4.6–2.6 ppm).

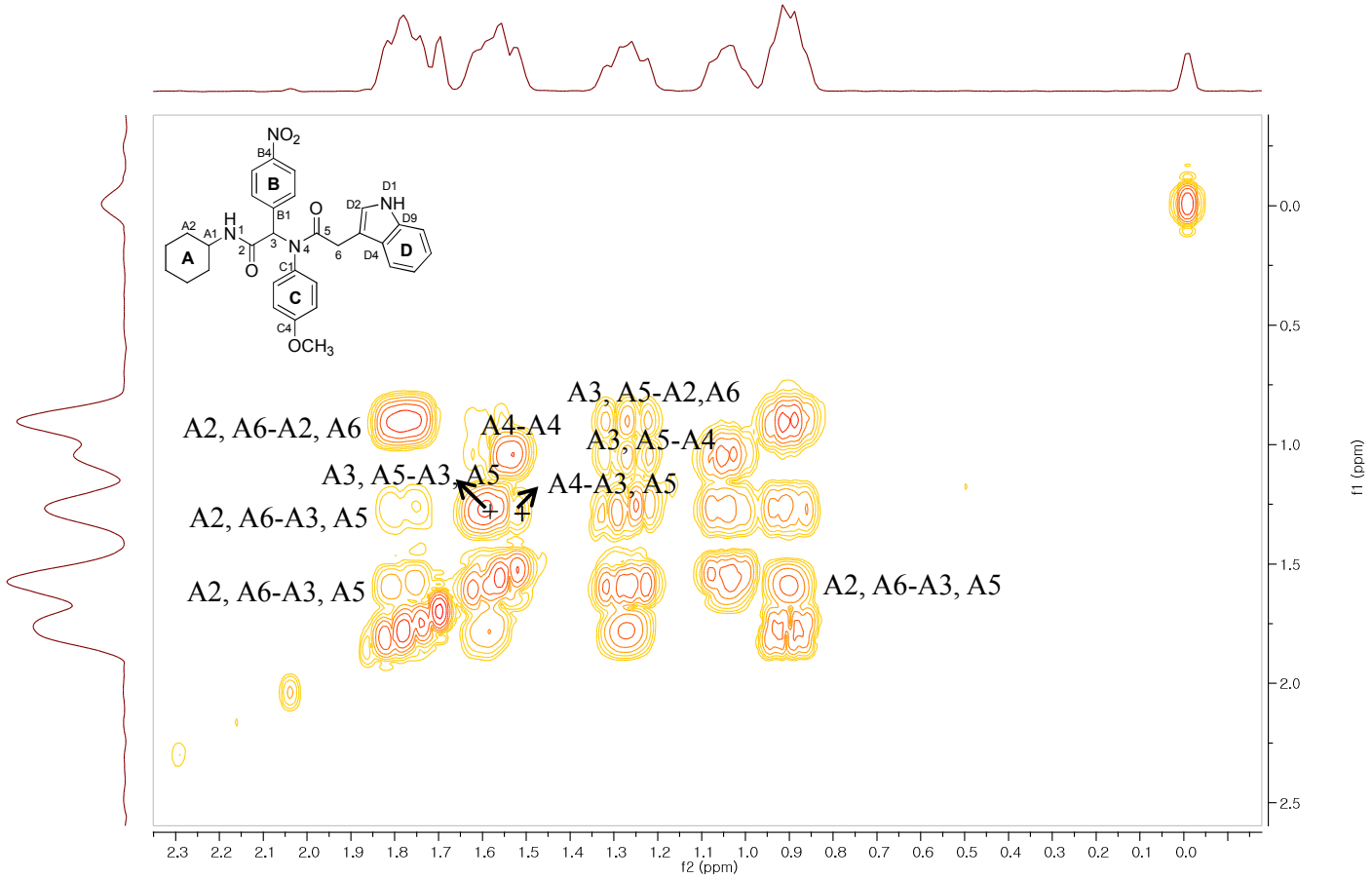

Figure S23. ^{1}H-^{1}H COSY (500, 500 MHz, $CDCl_3$) spectrum of **7** (2.3–0.0 ppm).

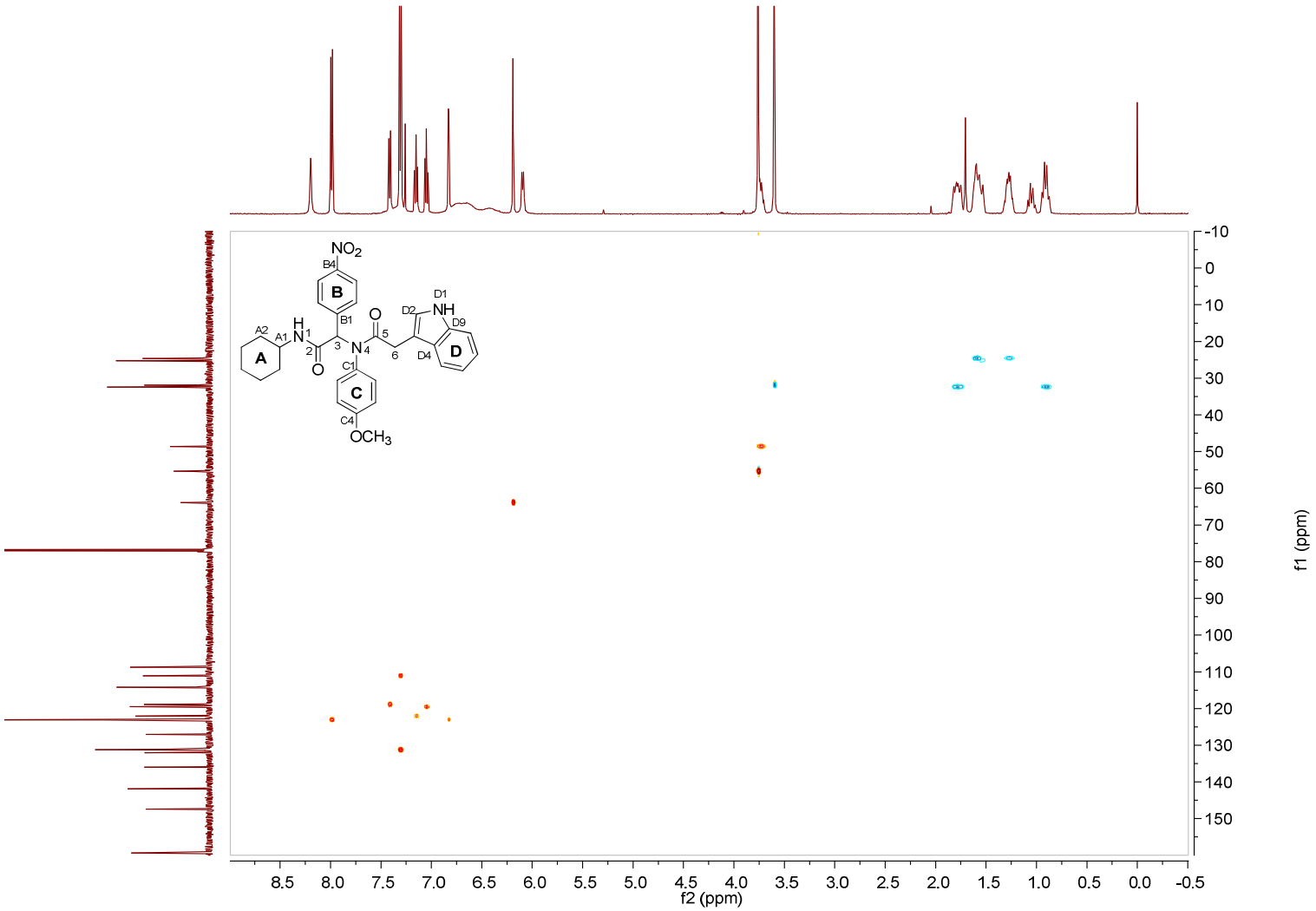

Figure S24. HSQC (500, 125 MHz, $CDCl_3$) spectrum of **7**.

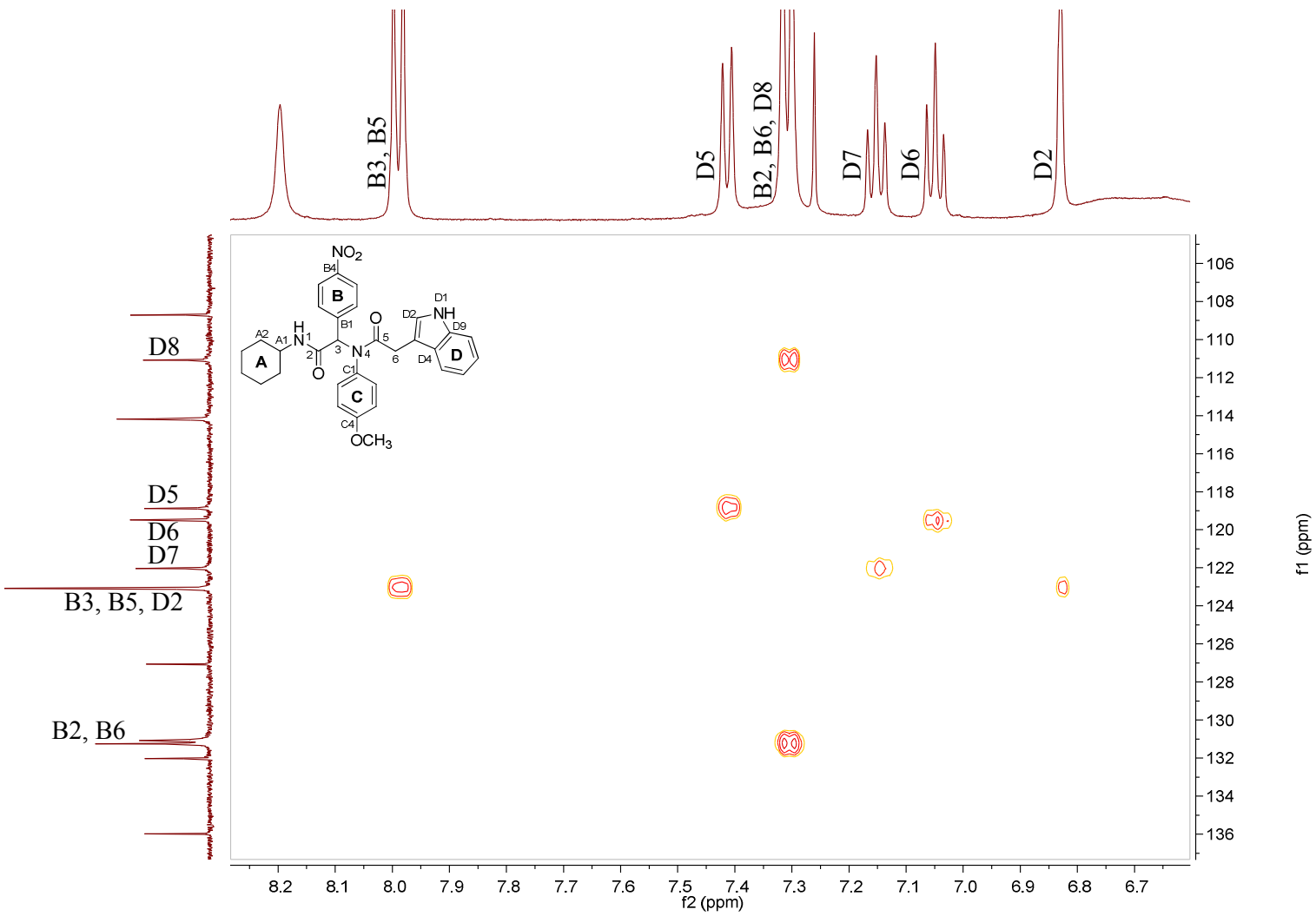

Figure S25. HSQC (500, 125 MHz, $CDCl_3$) spectrum of **7** (8.2–6.7 ppm).

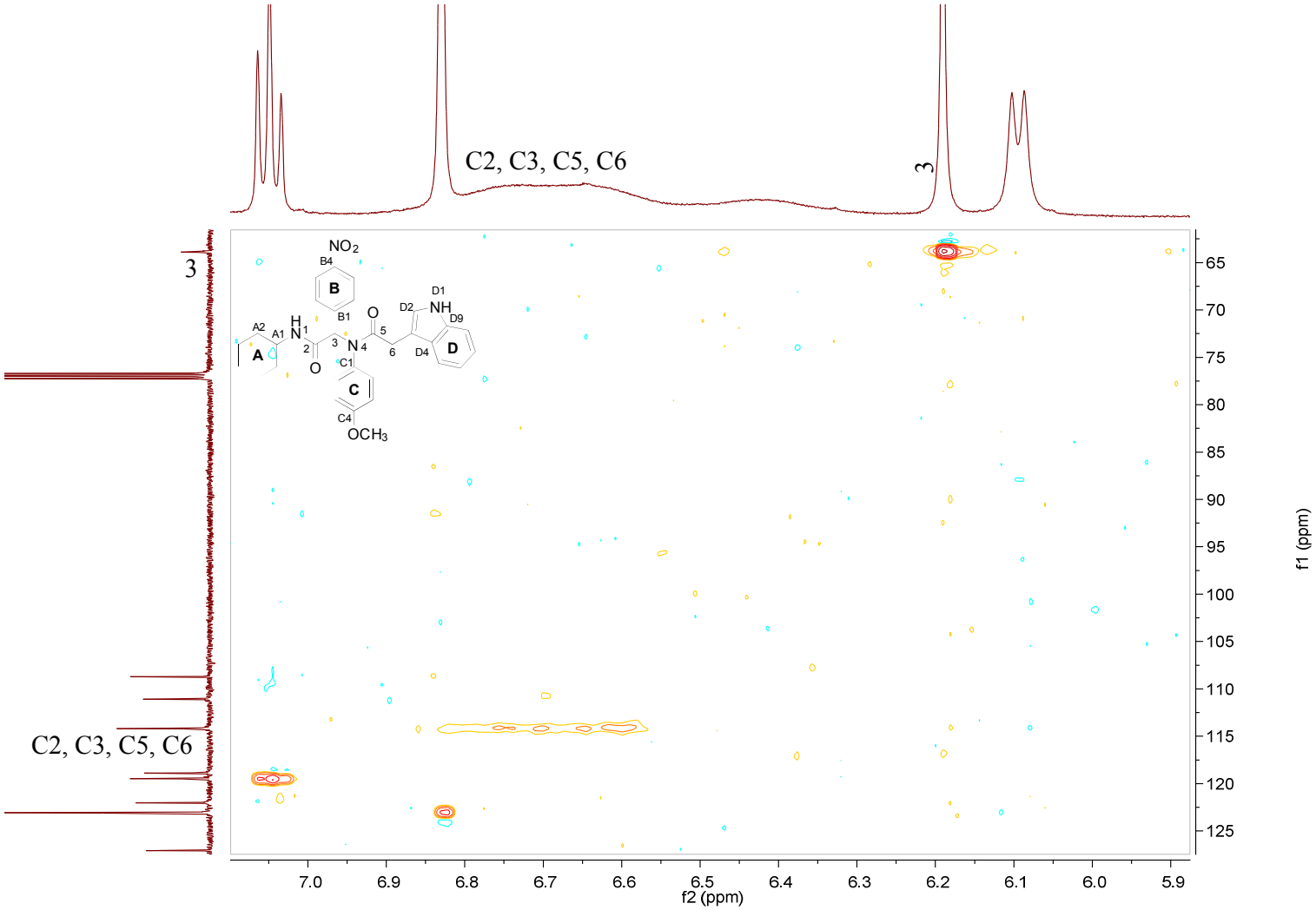

Figure S26. HSQC (500, 125 MHz, $CDCl_3$) spectrum of **7** (7.0–5.9).

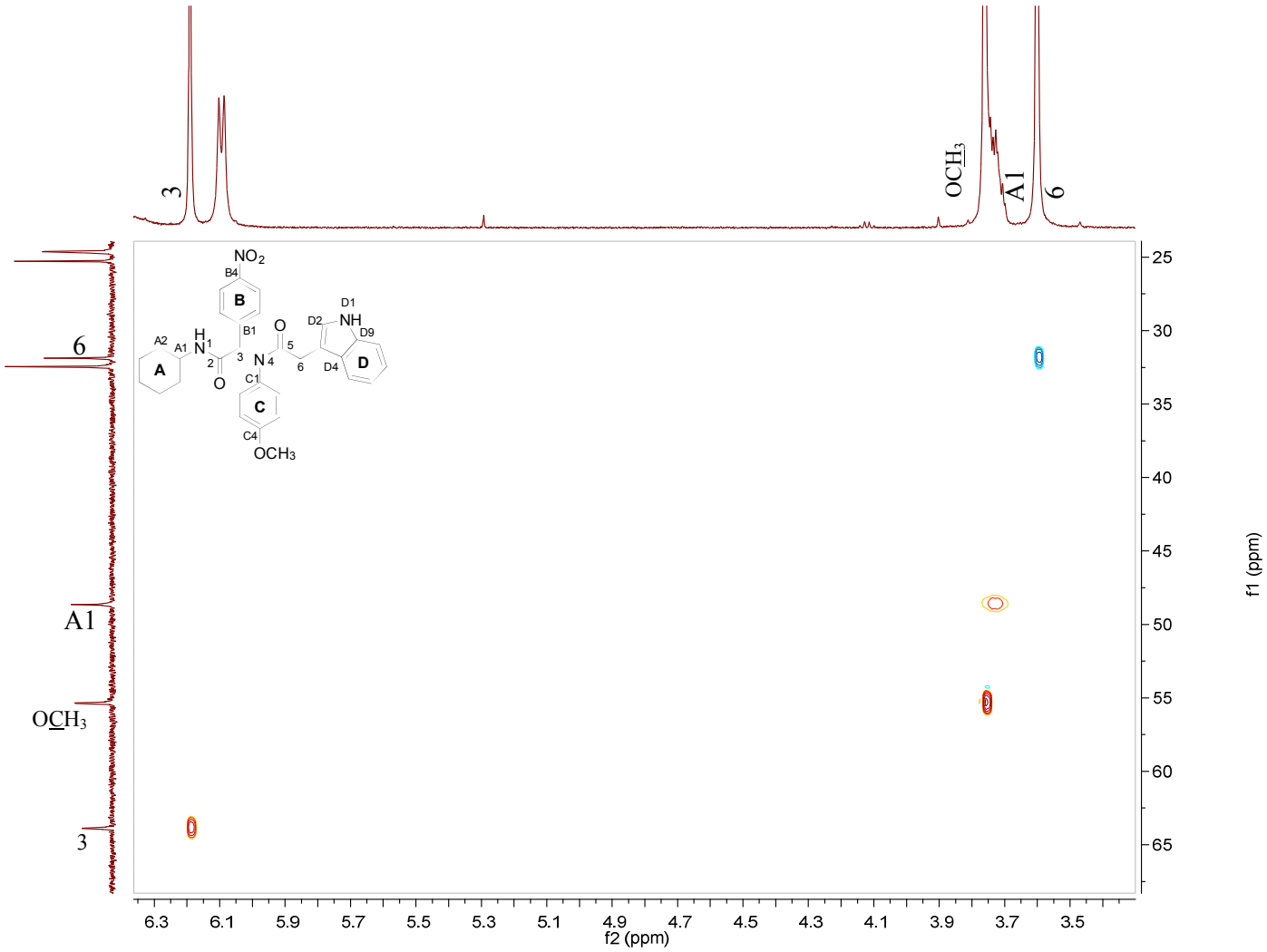

Figure S27. HSQC (500, 125 MHz, $CDCl_3$) spectrum of **7** (6.3–3.5 ppm).

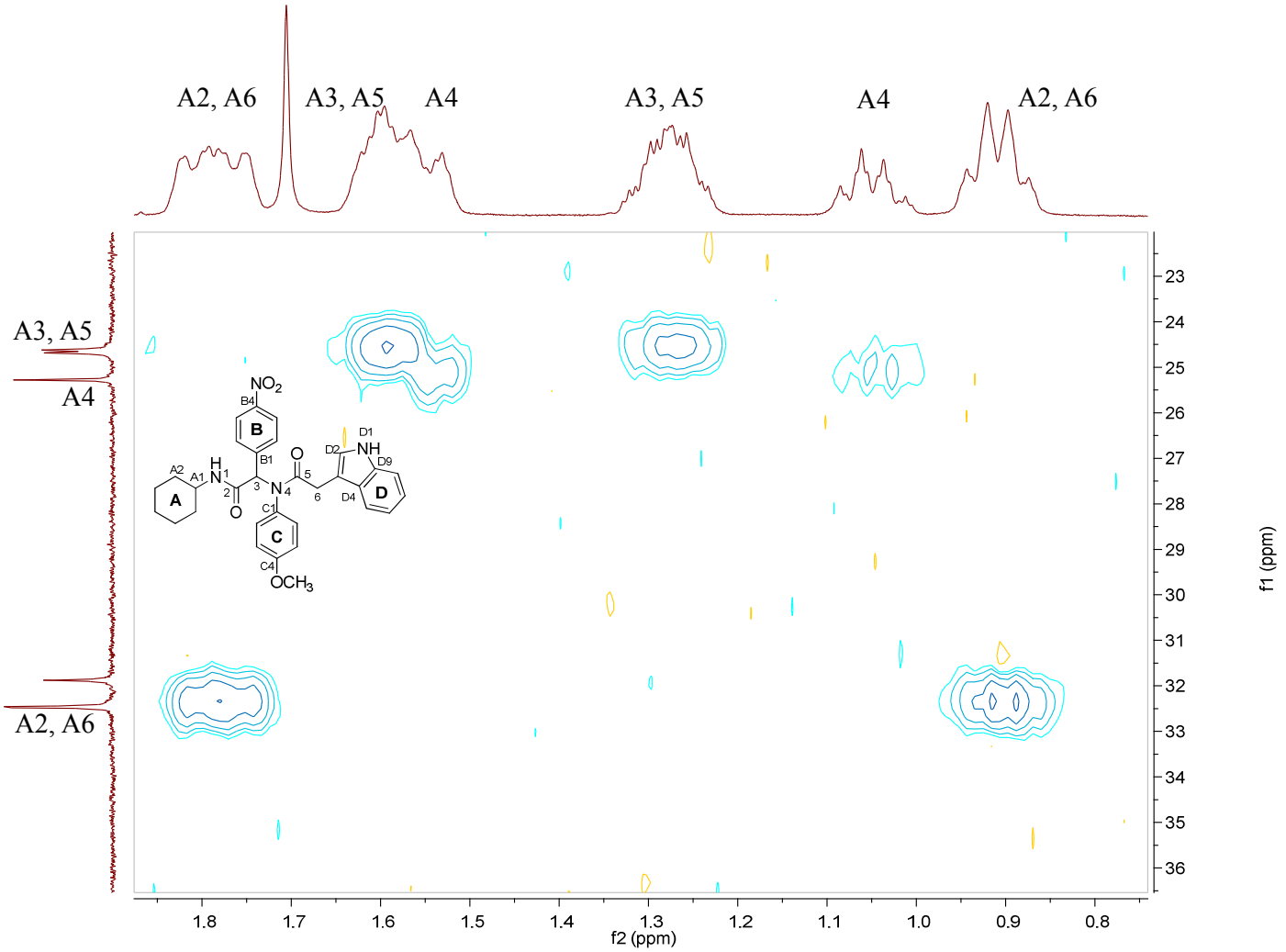

Figure S28. HSQC (500, 125 MHz, $CDCl_3$) spectrum of **7** (1.8–0.8 ppm).

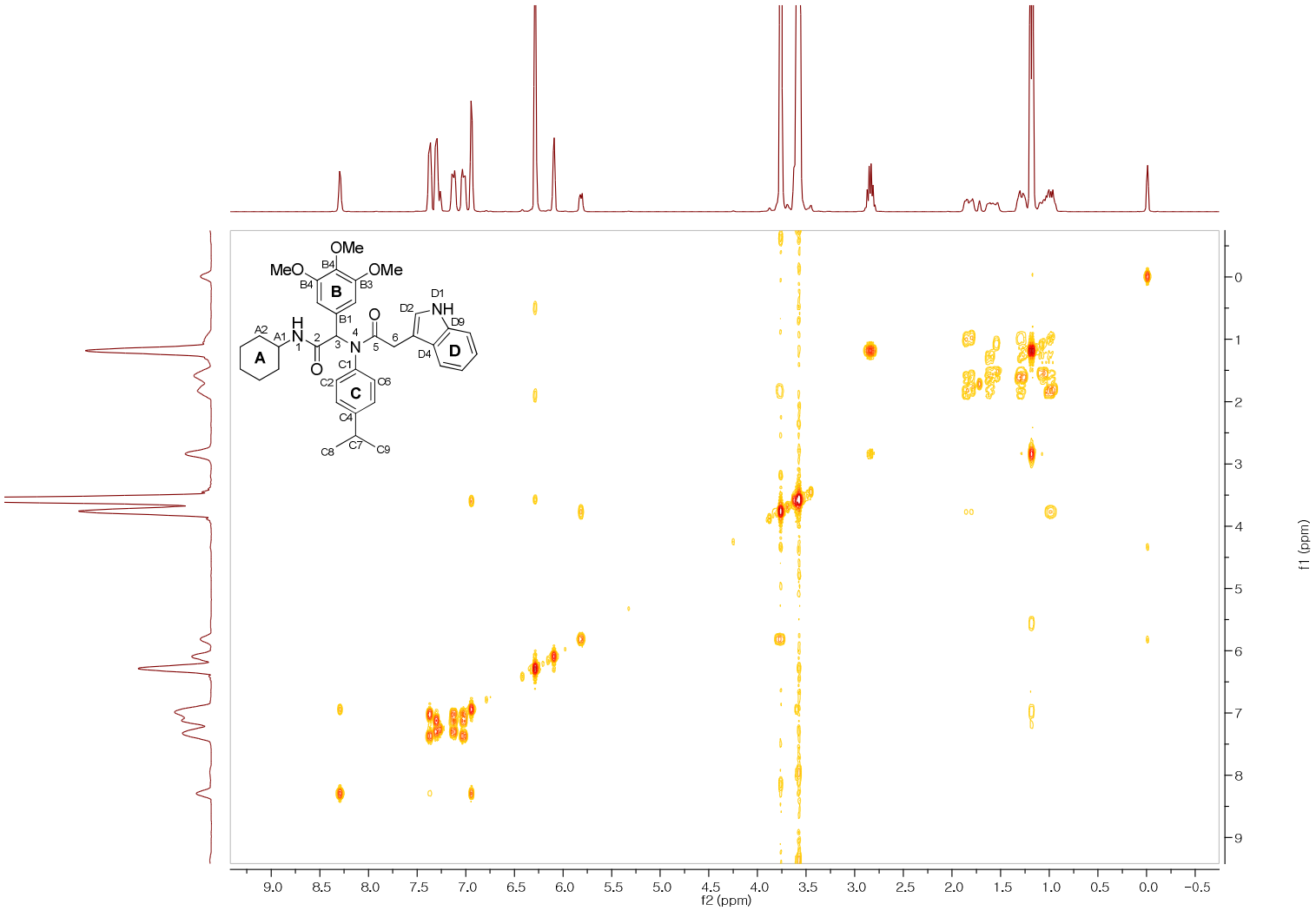

Figure S29. ^{1}H-^{1}H COSY (600, 600 MHz, $CDCl_3$) spectrum of **25**.

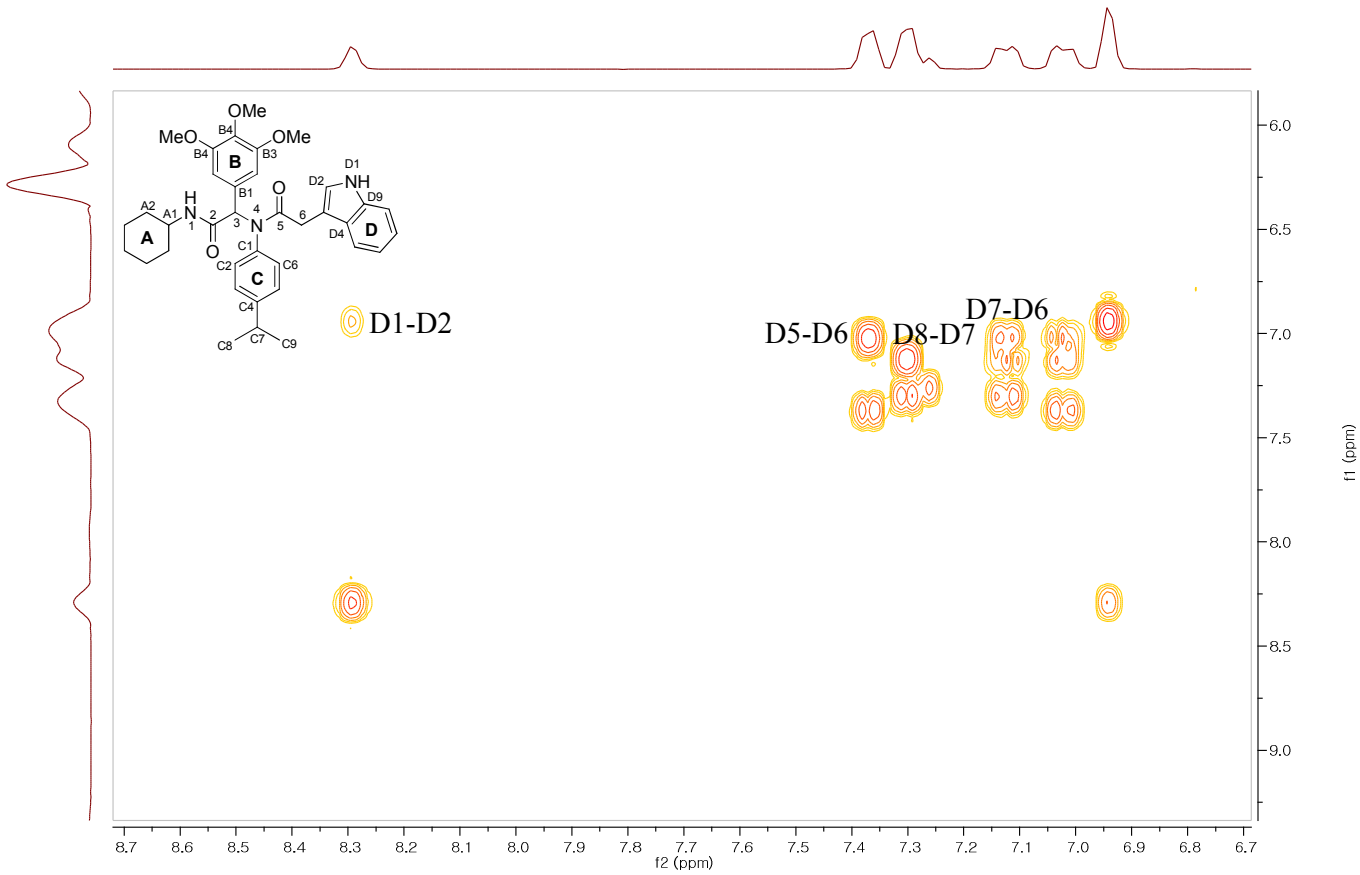

Figure S30. ^{1}H-^{1}H COSY (600, 600 MHz, $CDCl_3$) spectrum of **25** (8.7–6.7 ppm).

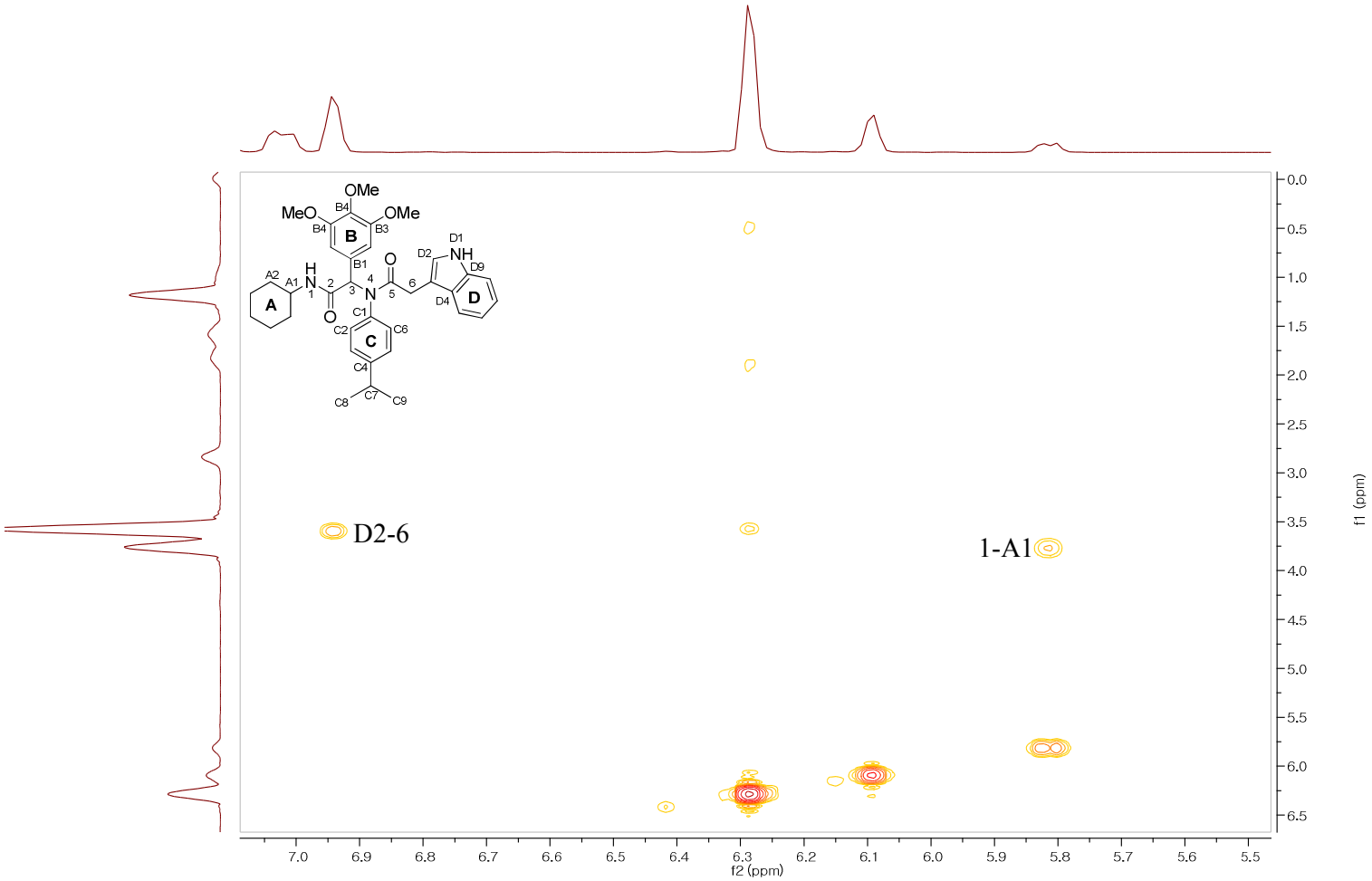

Figure S31. ^{1}H-^{1}H COSY (600, 600 MHz, $CDCl_3$) spectrum of **25** (7.0–5.5).

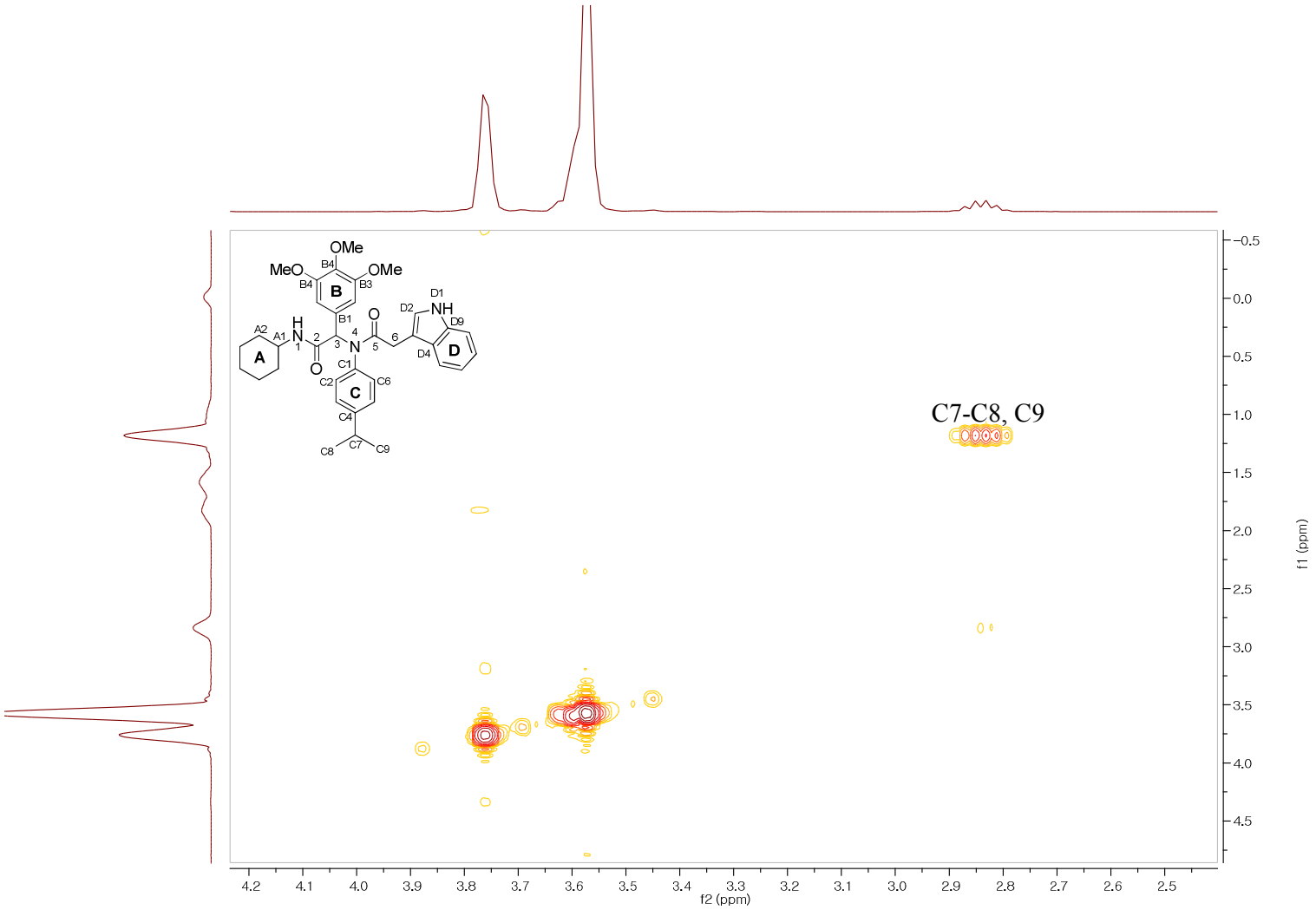

Figure S32. ^{1}H-^{1}H COSY (600, 600 MHz, $CDCl_3$) spectrum of **25** (4.2–2.5).

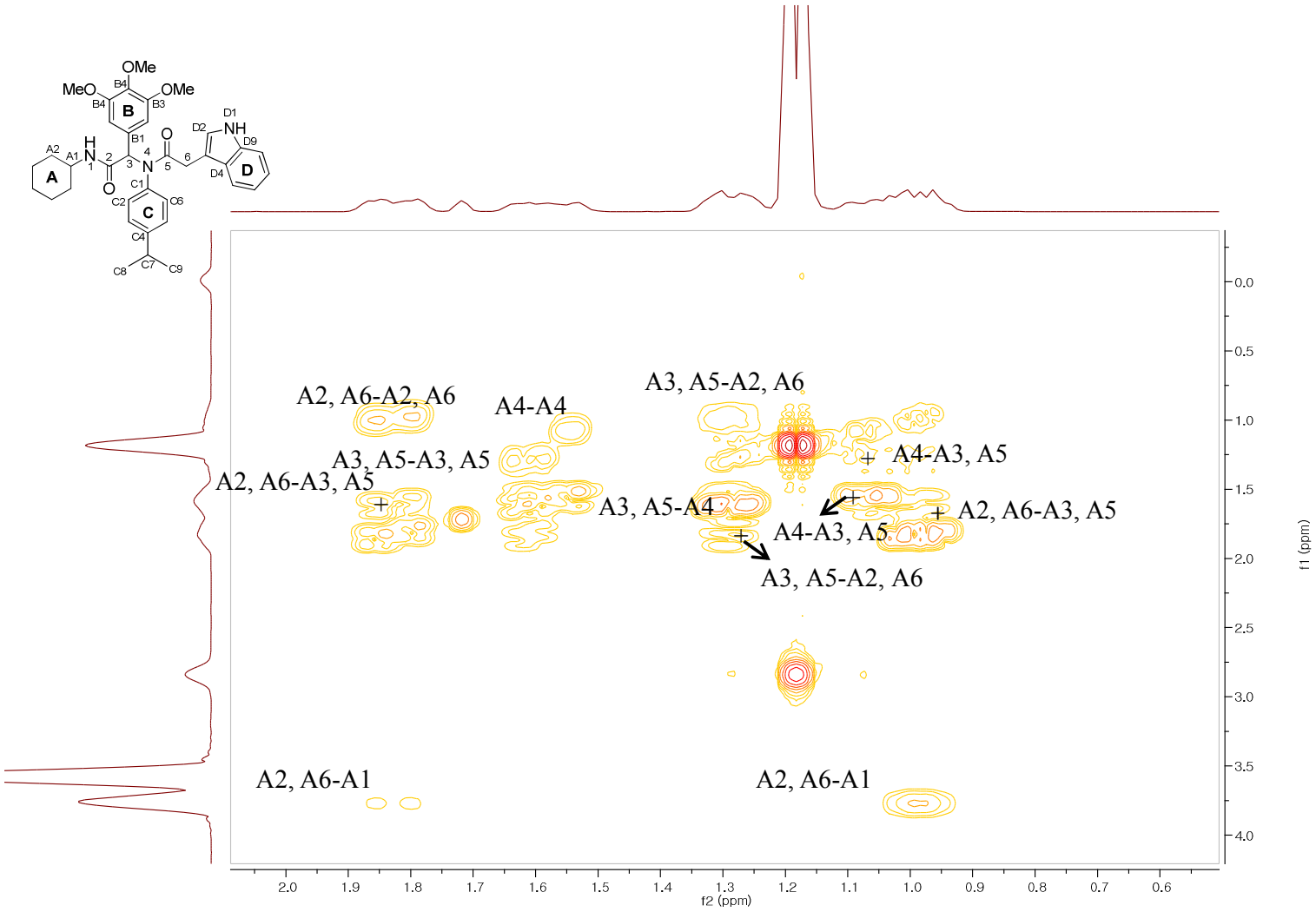

Figure S33. ^{1}H-^{1}H COSY (600, 600 MHz, $CDCl_3$) spectrum of **25** (2.0–0.6).

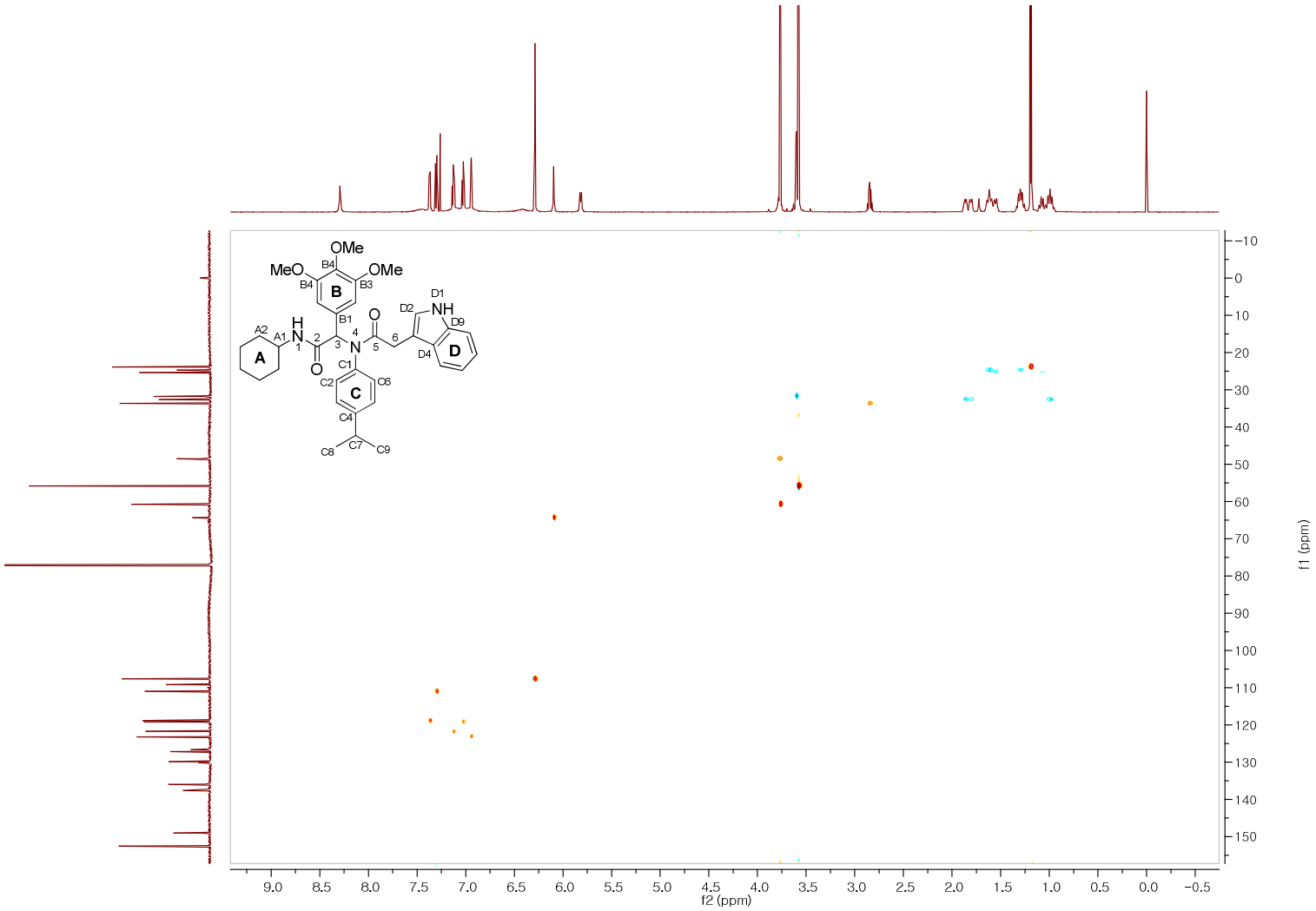

Figure S34. HSQC (600, 150 MHz, $CDCl_3$) spectrum of **25**.

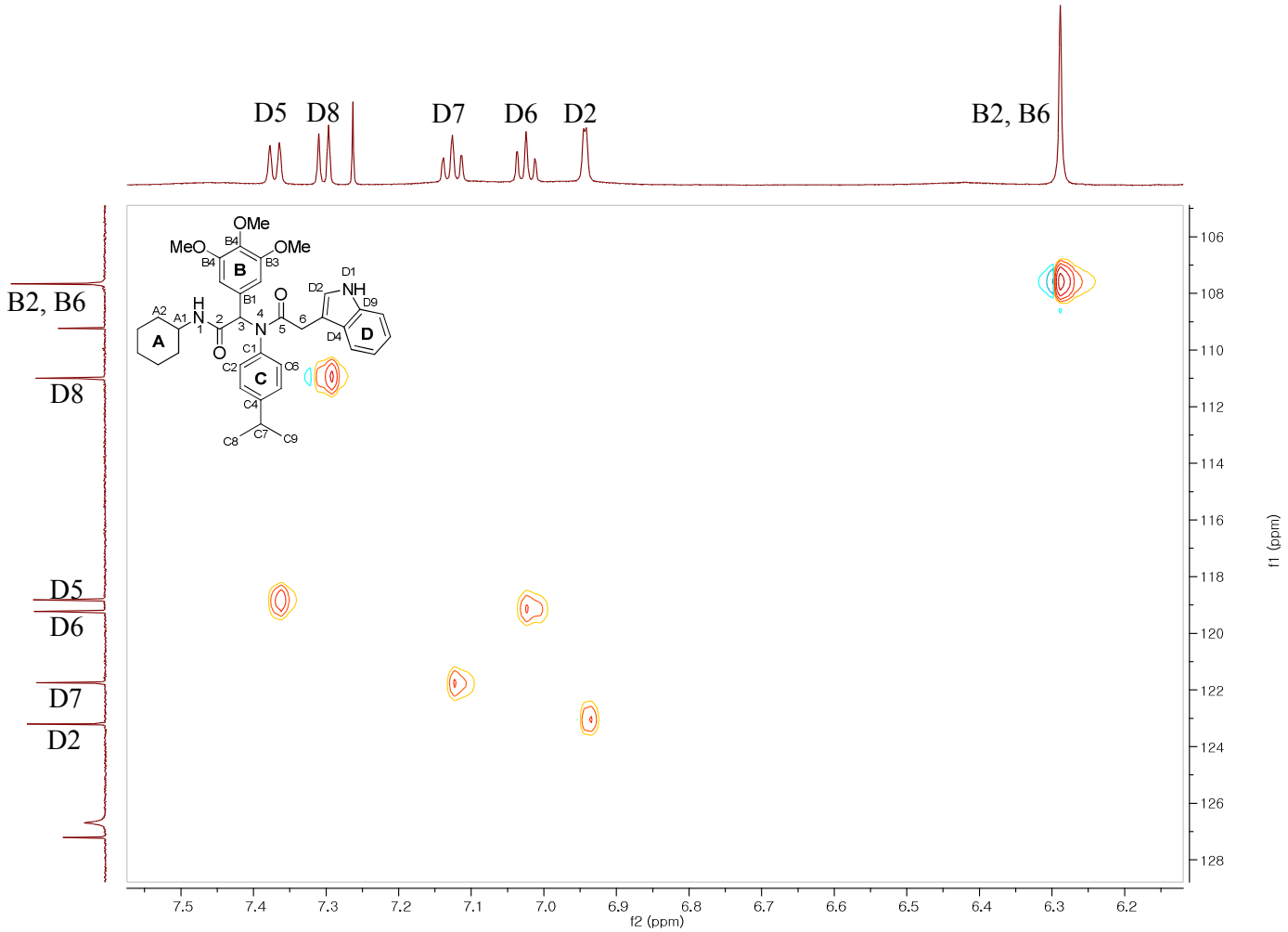

Figure S35. HSQC (600, 150 MHz, $CDCl_3$) spectrum of **25** (7.5–6.2 ppm).

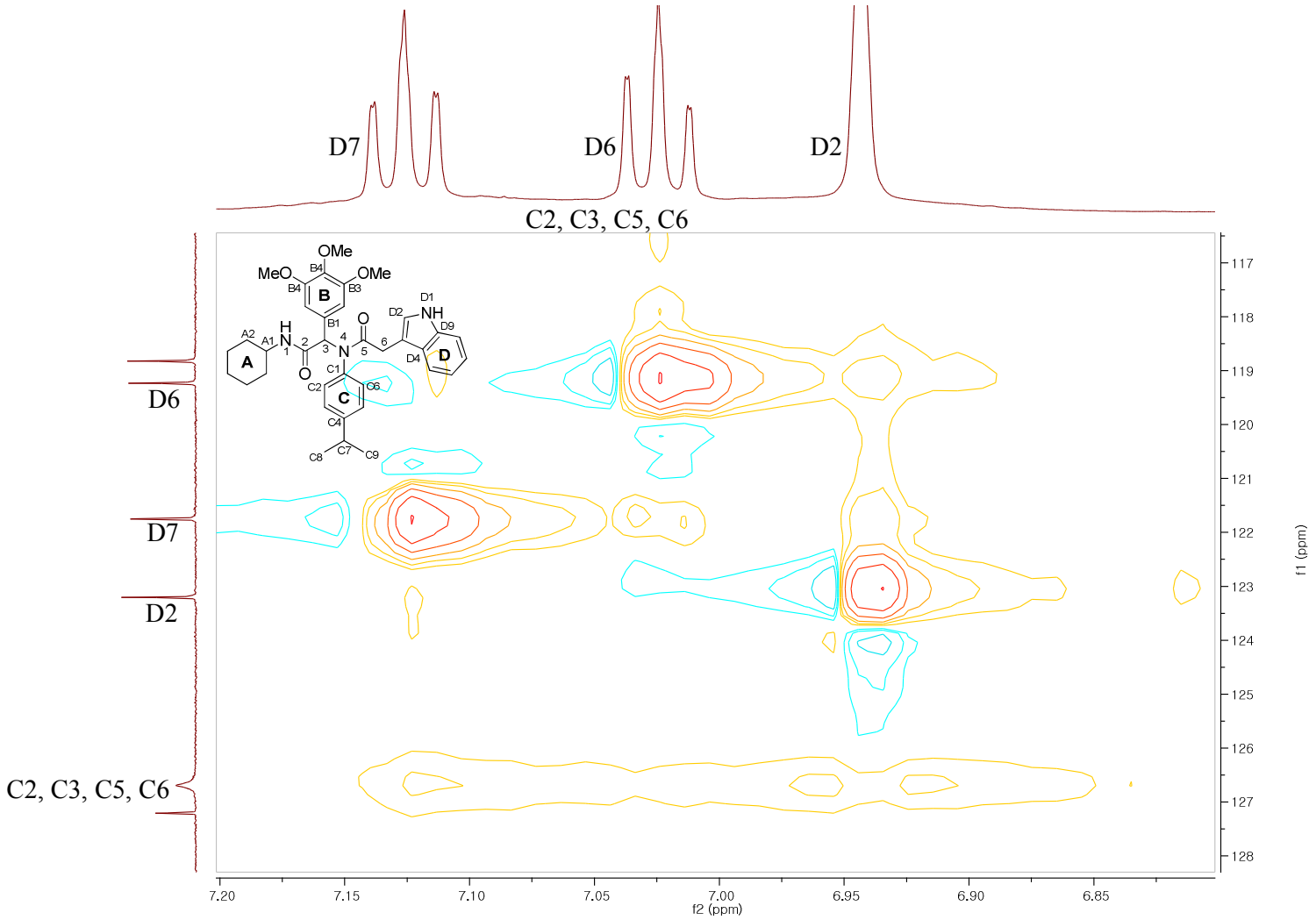

Figure S36. HSQC (600, 150 MHz, $CDCl_3$) spectrum of **25** (7.2–6.8 ppm).

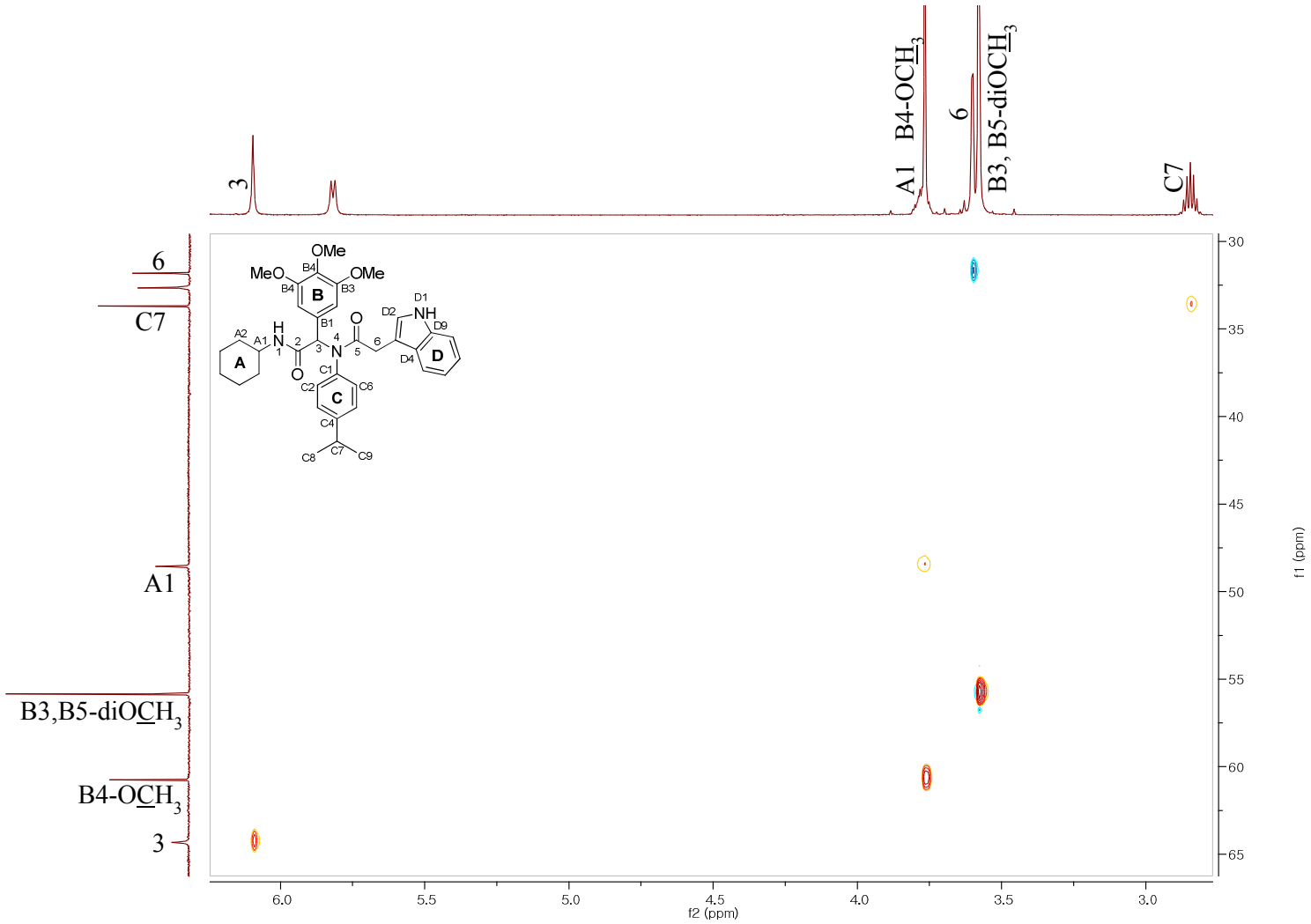

Figure S37. HSQC (600, 150 MHz, $CDCl_3$) spectrum of **25** (6.0–3.0 ppm).

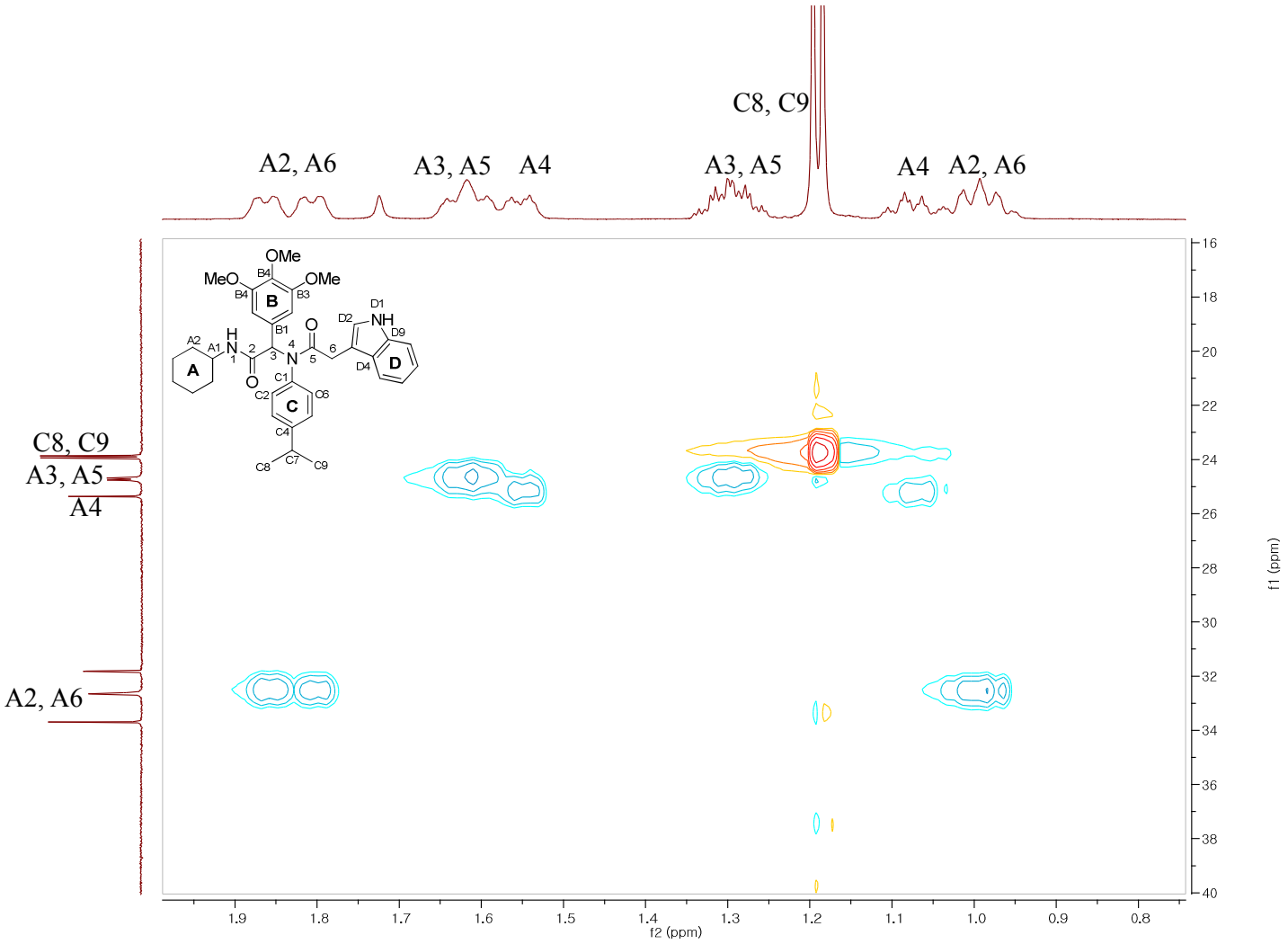

Figure S38. HSQC (600, 150 MHz, $CDCl_3$) spectrum of **25** (1.9–0.8 ppm).

References

(1) Hoel, A. M. L.; Nielsen, J. Microwave-assisted solid-phase Ugi four-component condensations. *Tetrahedron Letters* **1999**, *40*, 3941-3944.

(2) Cacalano, N. A.; Chen, B. X.; Cleveland, W. L.; Erlanger, B. F. Evidence for a functional receptor for cyclosporin A on the surface of lymphocytes. *Proc. Natl. Acad. Sci. U. S. A.* **1992**, *89*, 4353-4357.

(3) Song, F.; Zhang, X.; Ren, X. B.; Zhu, P.; Xu, J.; Wang, L.; Li, Y. F.; Zhong, N.; Ru, Q.; Zhang, D. W.; Jiang, J. L.; Xia, B.; Chen, Z. N. Cyclophilin A (CyPA) induces chemotaxis independent of its peptidylprolyl cis-trans isomerase activity: direct binding between CyPA and the ectodomain of CD147. *J. Biol. Chem.* **2011**, *286*, 8197-8203.

(4) Harvey, M. C., A. Fitting Models to Biological Data using Linear and Nonlinear Regression. A Practical Guide to Curve Fitting. **2004**.

(5) Kim, O. H.; Kim, Y. O.; Shim, J. H.; Jung, Y. S.; Jung, W. J.; Choi, W. C.; Lee, H.; Lee, S. J.; Kim, K. K.; Auh, J. H.; Kim, H.; Kim, J. W.; Oh, T. K.; Oh, B. C. beta-propeller phytase hydrolyzes insoluble Ca(2+)-phytate salts and completely abrogates the ability of phytate to chelate metal ions. *Biochemistry* **2010**, *49*, 10216-10227.